Electronic Supplementary Material (ESI) for Inorganic Chemistry Frontiers.

Supporting Information

Gating the photoactivity of the azobenzene-type ligands trapped within a dynamic system of M_4L_6 tetrahedral cage, an M_2L_2 metallocycle and mononuclear ML_n complexes

Piotr Cecot, Anna Walczak, Grzegorz Markiewicz, and Artur R. Stefankiewicz*

Table of Contents

Experimental Procedures

General

All chemicals and solvents were purchased from commercial sources and used as received. NMR spectra were acquired on Bruker Fourier 300 MHz, Bruker Avance IIIHD 400 MHz, Bruker Avance IIIHD 600 MHz or Bruker Avance III 700 MHz spectrometers and referenced on solvent residual peaks. Samples were irradiated directly in Quartz NMR tubes (Deutero GmbH, Qtz500-5-7),using a 4W UV lamp (λ_{max} = 365 nm). . ESI-MS spectra were recorded on a Bruker Impact HD Q-TOF spectrometer in positive ion mode. UV-Visible absorption spectra were collected using a Jasco V-750 spectrophotometer in the 200–700 nm wavelength range, in Hellma Quarz Suprasil cuvettes, of 1 mm path length. Samples were irradiated using a 1 W Cree LED (λ_{max} = 395 nm).

Synthetic procedures

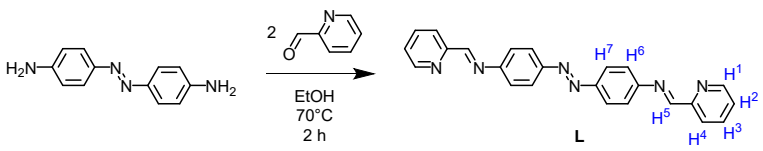

Scheme S1. Ligand *trans*-**L** synthesis.

trans-***L***: *trans*-4,4'-diaminoazobenzene (106.1 mg, $5.0 \cdot 10^{-4}$ mol) was added to 2.5 mL of anhydrous ethanol and the thus obtained suspension was heated to 80°C. Then, 2-pyridinecarboxaldehyde (95.1 µL, $1.0 \cdot 10^{-3}$ mol) was added to boiling mixture as a solution in 2.5 mL of anhydrous ethanol. After 2 h the mixture was cooled to room temperature. The orange precipitate was filtered off, washed with cold anhydrous ethanol and acetonitrile and was dried in vacuo. Yield = 82 %

^{1}H NMR (300 MHz, Chloroform-*d*) δ 8.75 (d, J = 4.7 Hz, 2H), 8.67 (s, 2H), 8.24 (d, J = 7.9 Hz, 2H), 8.01 (d, J = 8.6 Hz, 4H), 7.85 (td, J = 7.7, 1.6 Hz, 2H), 7.41 (td, J = 6.5, 5.9, 1.4 Hz, 6H) ppm. ^{13}C NMR (75 MHz, Chloroform-*d*) δ 161.49, 154.41, 153.34, 151.39, 149.99, 136.91, 125.57, 124.24, 122.31, 122.02 ppm. ^{1}H NMR (300 MHz, Acetonitrile-d_3) δ 8.75 (s, 2H), 8.69 (s, 2H), 8.24 (d, J = 7.7 Hz, 2H), 8.03 (d, J = 8.3 Hz, 3H), 7.99 – 7.89 (m, 2H), 7.50 (d, J = 8.4 Hz, 6H) ppm.

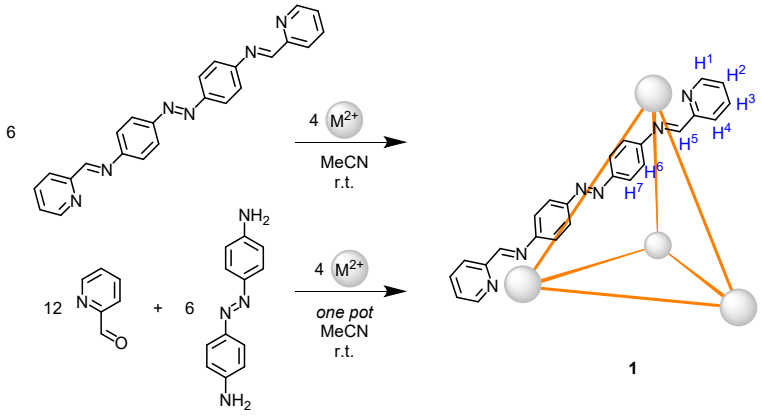

Scheme S2. $[M_4L_6](anion)_8$ cage synthesis.

*[Zn$_4$**L**$_6$](NTf$_2$)$_8$*: *trans*-**L** (5.0 mg, 1.28·10^{-5} mol) was suspended in 2.5 mL of acetonitrile and then Zn(NTf$_2$)$_2$ (5.6 mg, 8.96·10^{-6} mol) was added as a solution in 2.5 mL of acetonitrile. Thus obtained clear solution was stirred for 1 h at RT. The product was precipitated by addition of Et$_2$O, isolated by centrifugation followed by washing with diethyl ether and chloroform, and drying in vacuo. ^{1}H NMR (600 MHz, Acetonitrile-d_3) δ 8.85 (s, 2H), 8.71 (s, 3H), 8.56 – 8.46 (m, 11H), 8.40 (d, J = 7.7 Hz, 2H), 8.34 (d, J = 7.6 Hz, 3H), 8.22 (d, J = 7.6 Hz, 3H), 8.07 (d, J = 4.6 Hz, 2H), 7.97 (d, J = 5.1 Hz, 4H), 7.90 (dd, J = 23.3, 3.9 Hz, 15H), 7.86 – 7.80 (m, 9H), 6.70 (d, J = 8.6 Hz, 4H), 6.45 (d, J = 8.7 Hz, 4H), 6.30 (d, J = 8.7 Hz, 4H).
*[Zn$_4$**L**$_6$](NTf$_2$)$_8$ one-pot*: *trans*-4,4'-diaminoazobenzene (2.7 mg, 1.28·10^{-5} mol) and Zn(NTf$_2$)$_2$ (5.6 mg, 8.96·10^{-6} mol) were added to the NMR tube and dissolved in 0.3 mL of acetonitrile-d_3. 2-pyridinecarboxaldehyde (2.43 µL, 2.56·10^{-5} mol) was dissolved in 0.3 mL of acetonitrile-d_3 and then added to the solution in the NMR tube. The reaction mixture was sonicated for 15 min and characterized without isolation. ^{1}H NMR (300 MHz, Acetonitrile-d_3) δ 8.79 (s, 1H), 8.68 (s, 2H), 8.47 (q, J = 8.3 Hz, 8H), 8.34 (dd, J = 16.7, 7.6 Hz, 2H), 8.18 (d, J = 7.2 Hz, 1H), 8.04 (d, J = 4.8 Hz, 2H), 7.89 (s, 1*3*8H), 7.91 – 7.74 (m, 5H), 6.67 (d, J = 8.3 Hz, 2H), 6.42 (d, J = 7.9 Hz, 3H), 6.27 (d, J = 8.2 Hz, 2H).
*[Fe$_4$**L**$_6$](OTf)$_8$ one-pot*: Reaction was conducted under Ar atmosphere to prevent Fe^{2+} oxidation. 4,4'-diaminoazobenzene (2.7 mg, 1.28·10^{-5} mol) and Fe(OTf)$_2$ (5.6 mg, 8.96·10^{-6} mol) were dissolved in 0.6 mL of degassed acetonitrile-*d3 and then* 2-pyridinecarboxaldehyde (2.43 µL, 2.56·10^{-5} mol) was added. The deep violet solution was sonicated for 15 min and characterized without isolation. ^{1}H NMR (600 MHz, Acetonitrile-d_3) δ 9.16 – 8.87 (m, 1H), 8.71 – 8.52 (m, 1H), 8.42 (q, *J* = 7.3 Hz, 1H), 7.94 – 7.72 (m, 3H), 7.53 – 7.37 (m, 1H), 5.73 – 5.50 (m, 2H).

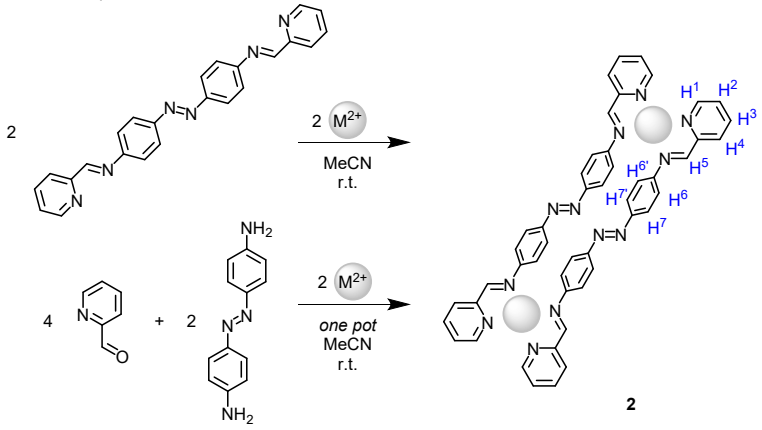

Scheme S3. $[M_2L_2](anion)_4$ metallocycle synthesis.

*[Zn$_2$**L**$_2$](NTf$_2$)$_4$*: *trans*-**L** (10.1 mg, 2.59·10^{-5} mol) was suspended in 2.5 mL of acetonitrile and then Zn(NTf$_2$)$_2$ (18.8 mg, 3.00·10^{-5} mol) was added as a solution in 2.5 mL of acetonitrile. Thus obtained clear solution was stirred for 1 h at RT. The product was precipitated by addition of Et$_2$O, isolated by centrifugation followed by washing with diethyl ether and chloroform, and drying *in vacuo*. ^{1}H NMR (300 MHz, Acetonitrile-d_3) δ 8.73 (s, 1H), 8.45 – 8.13 (m, 2H), 7.97 (dq, J = 20.7, 10.7, 8.3 Hz, 4H), 7.15 (t, J = 6.8 Hz, 2H).
*[Cd$_2$**L**$_2$](ClO$_4$)$_4$*: *trans*-**L** (10.0 mg, 2.56·10^{-5} mol) was suspended in 2.5 mL of acetonitrile and then Cd(ClO$_4$)·6 H$_2$O (14.3 mg, 2.56·10^{-5} mol) was added as a solution in 1.0 mL of acetonitrile. Thus obtained clear solution was stirred for 1 h at RT. The product was precipitated by addition of Et$_2$O, isolated by centrifugation followed by washing with diethyl ether and chloroform, and drying *in vacuo*. ^{1}H NMR (300 MHz, Acetonitrile-d_3) δ 8.90 (s, 2H), 8.68 (s, 0H), 8.25 – 8.10 (m, 1H), 7.89 (s, 4H), 7.23 (s, 2H), 6.88 (s, 1H), 6.67 (s, 1H).

Results

Characterization

Ligand

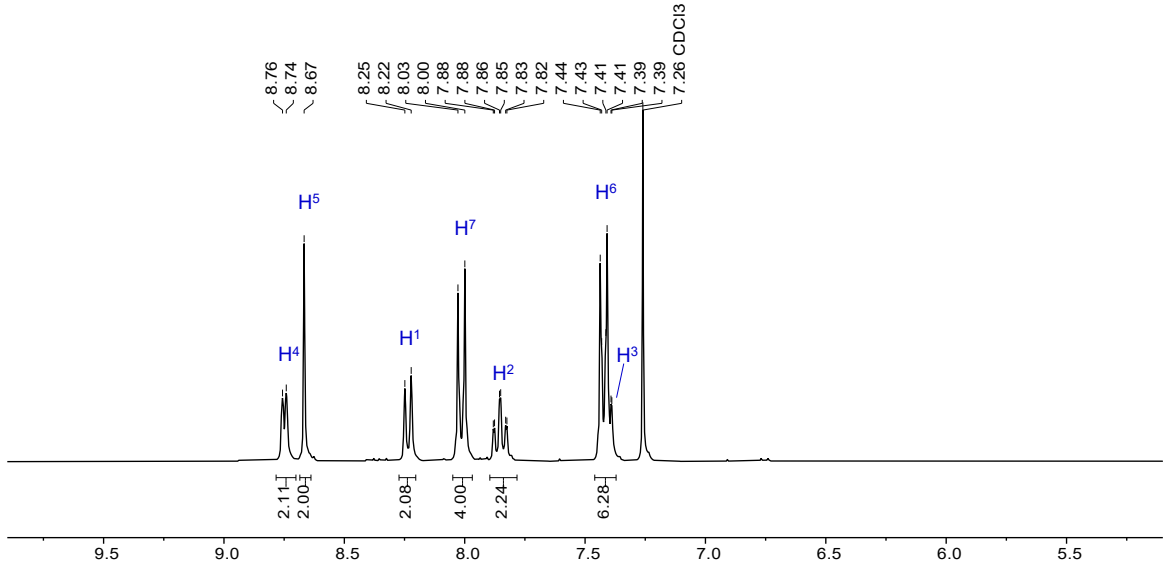

Figure S1. ^{1}H NMR (300 MHz, $CDCl_3$) spectrum of *trans*-**L**.

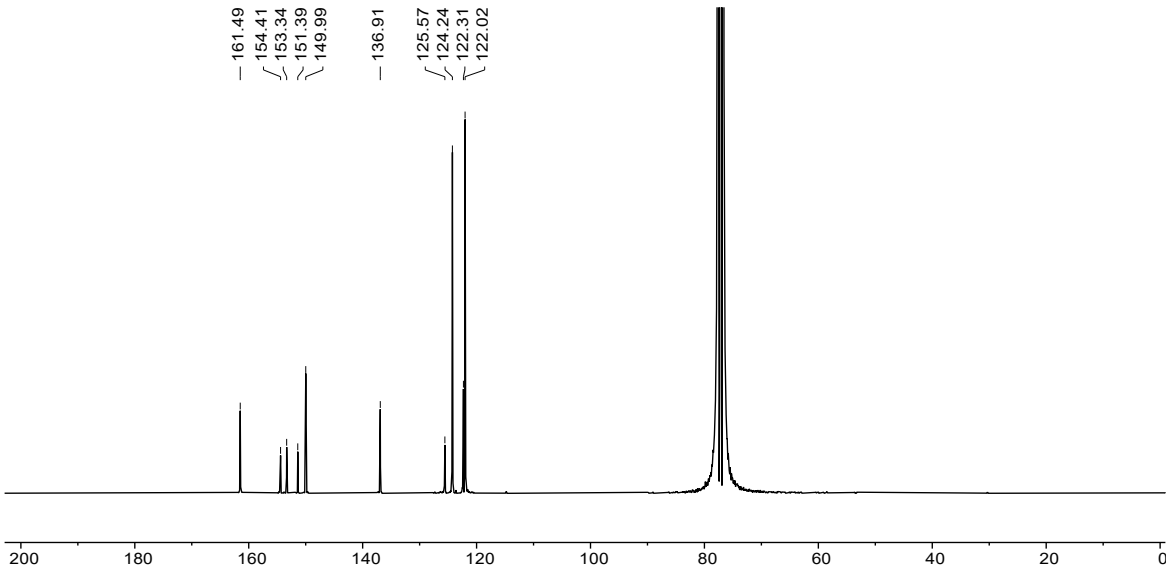

Figure S2. ^{13}C NMR (75MHz, $CDCl_3$) spectrum of *trans*-**L**.

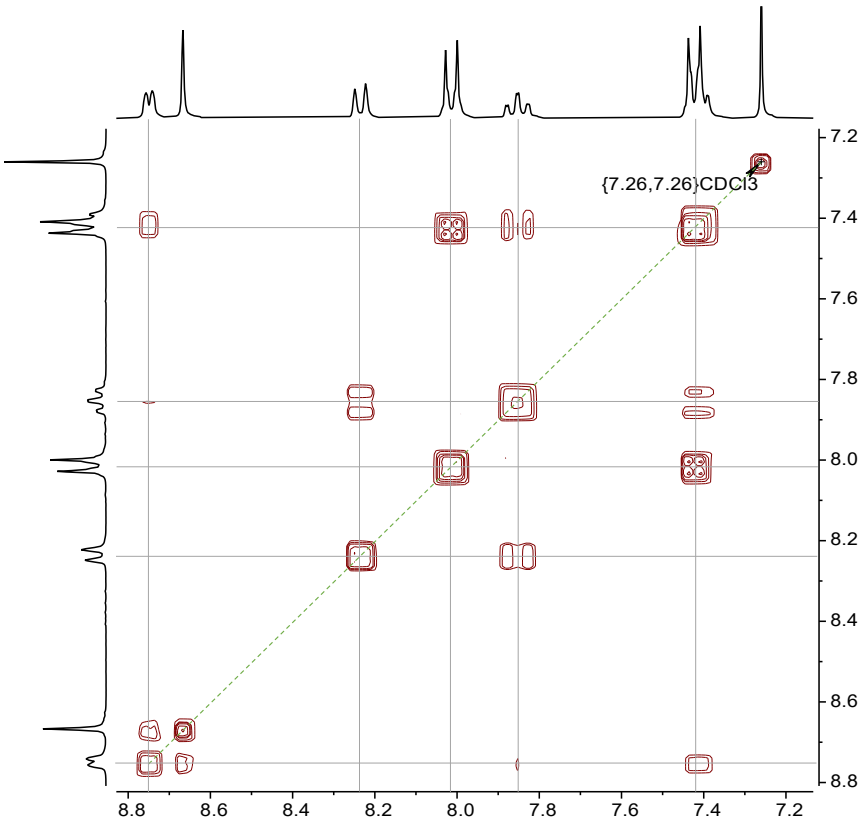

Figure S3. COSY (300 MHz, $CDCl_3$) spectrum of *trans*-**L**.

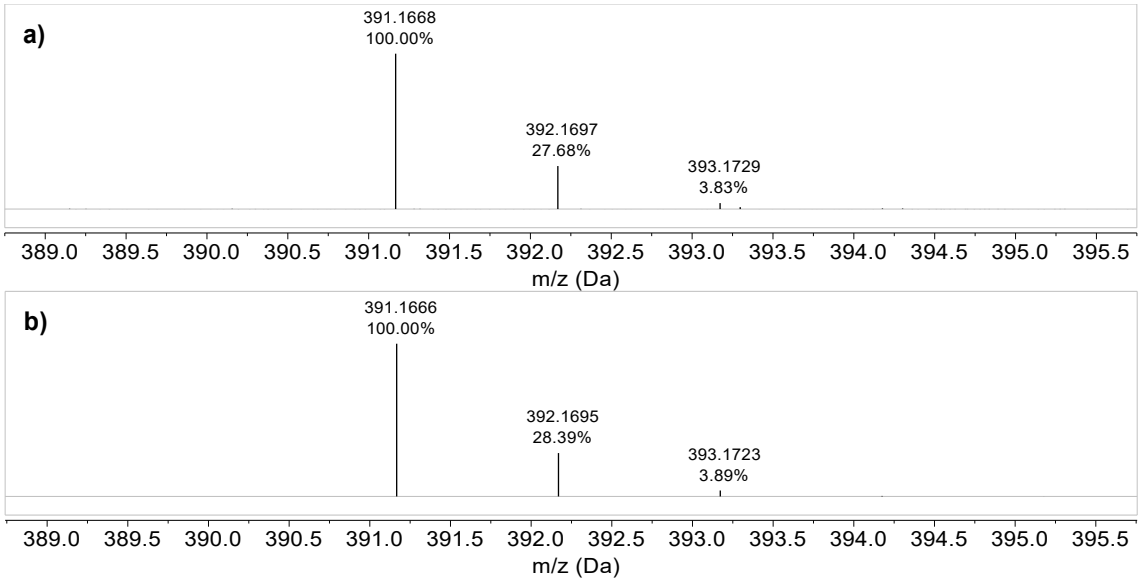

Figure S4. ESI-MS spectrum of *trans*-**L** a) experimental, b) calculated for $[M+H]^+$.

$[Zn_4L_6](NTf_2)_8$ Tetrahedral cage

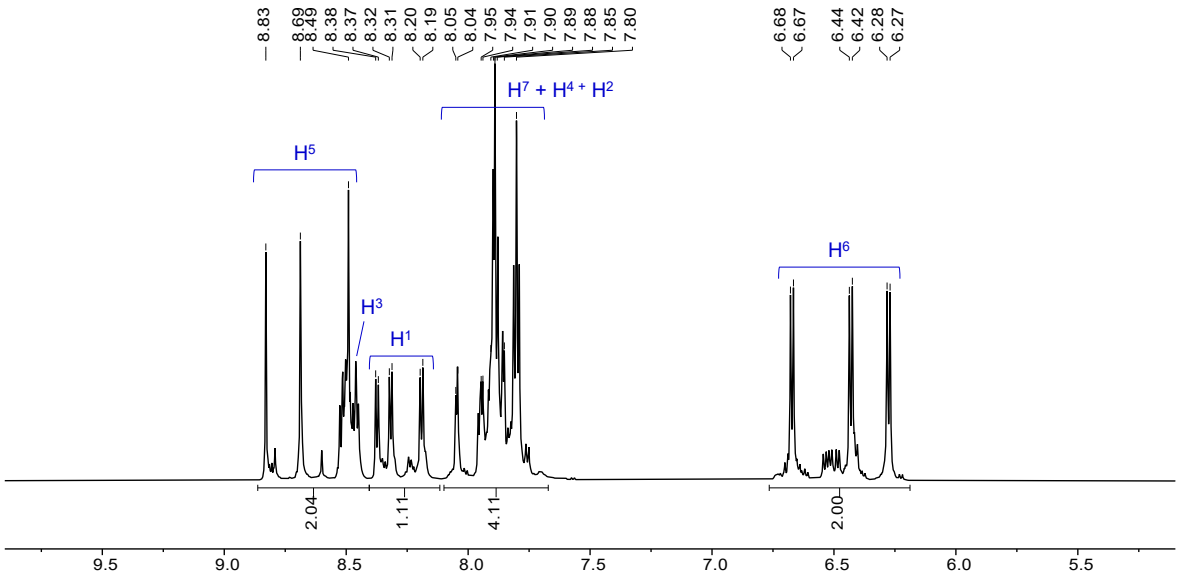

Figure S5. ^{1}H NMR (700 MHz, CD_3CN) spectrum of tetrahedral cage $[Zn_4L_6](NTf_2)_8$.

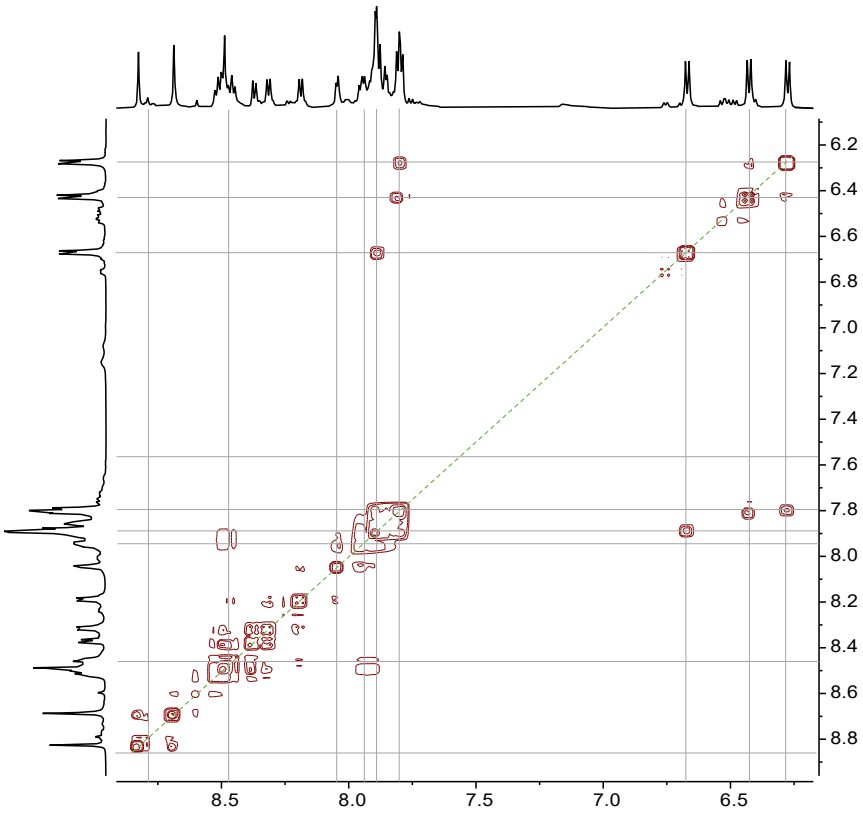

Figure S6. COSY (600 MHz, CD_3CN) spectrum of tetrahedral cage $[Zn_4L_6](NTf_2)_8$.

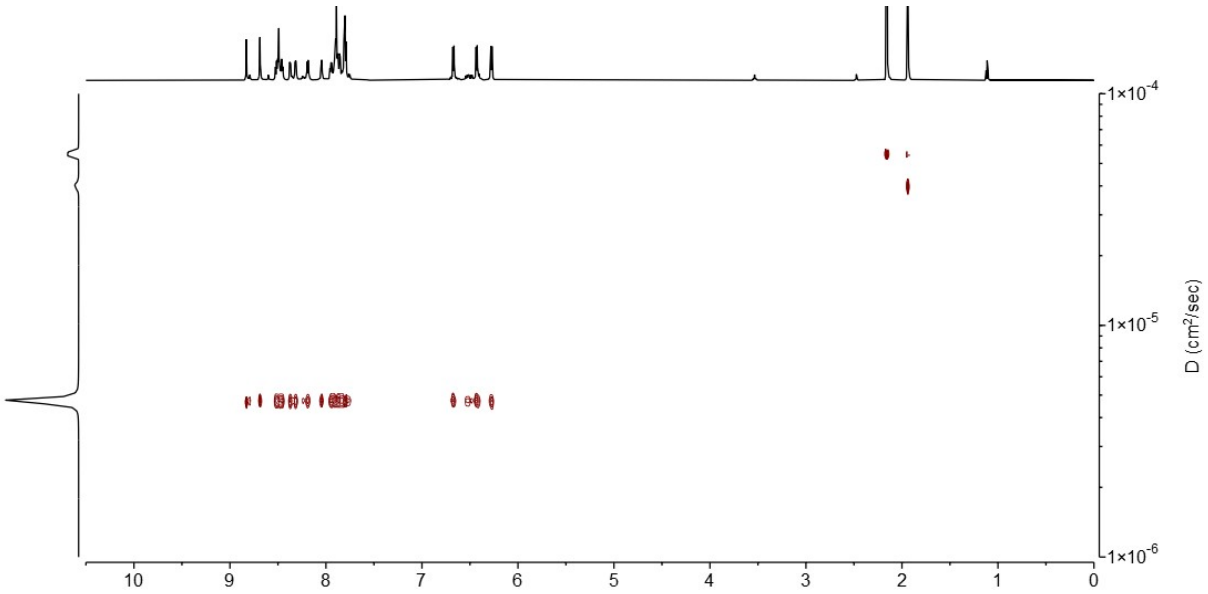

Figure S7. DOSY (700 MHz, 298K, CD_3CN) spectrum of tetrahedral cage $[Zn_4\mathbf{L}_6](NTf_2)_8$.

$[Fe_4\mathbf{L}_6](OTf)_8$ Tetrahedral cage

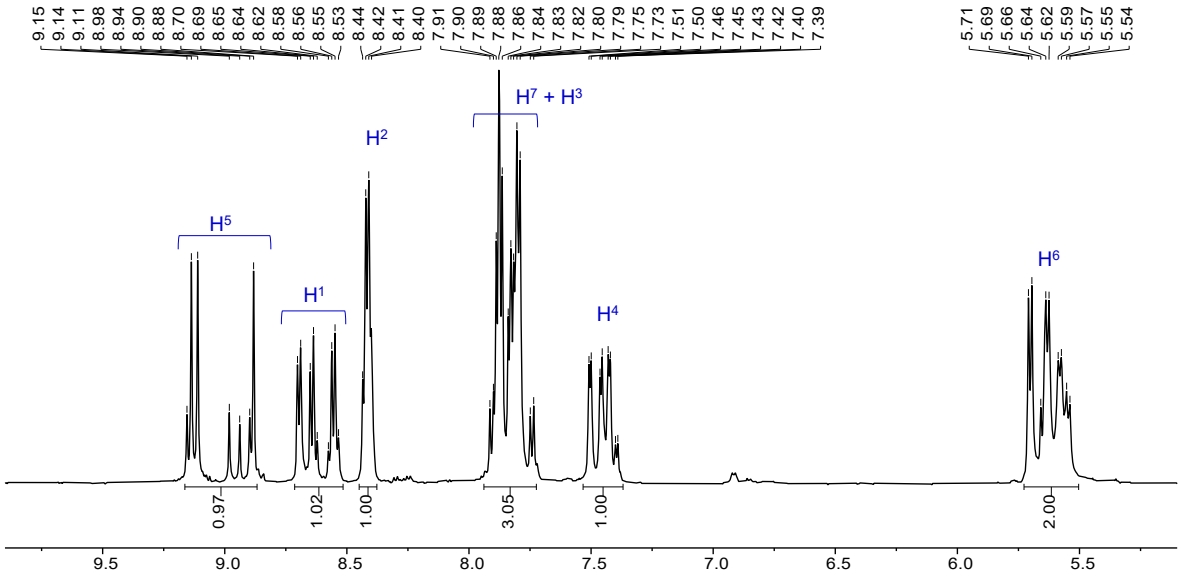

Figure S8. ^1H NMR (600 MHz, CD_3CN) spectrum of tetrahedral cage $[Fe_4\mathbf{L}_6](OTf)_8$.

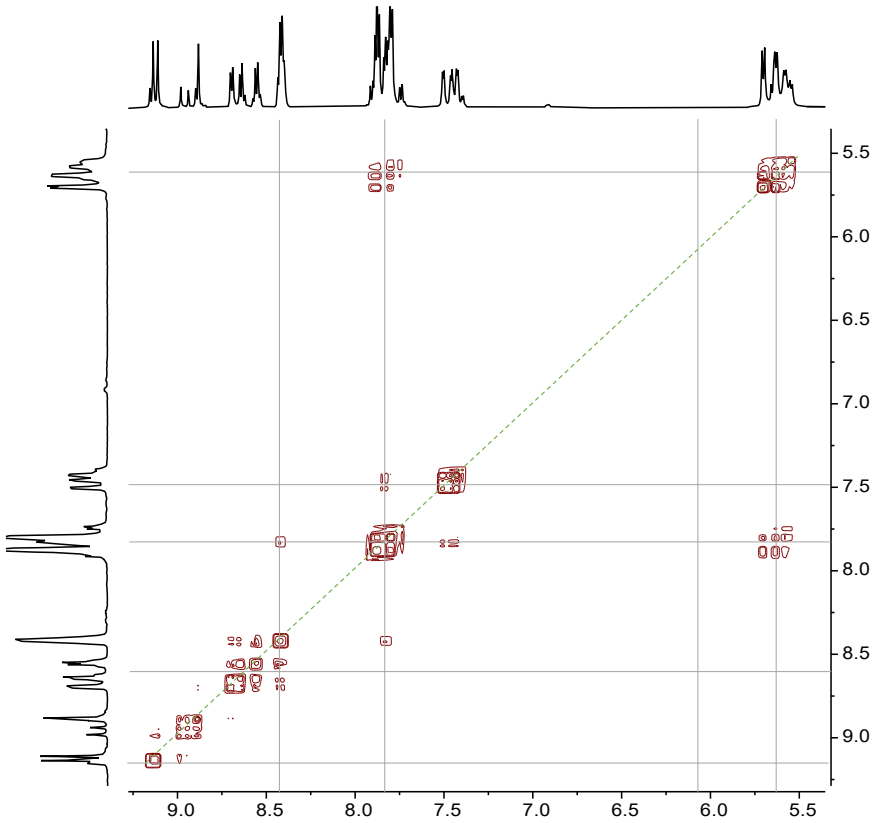

Figure S9. COSY (600 MHz, CD_3CN) spectrum of tetrahedral cage $[Fe_4\mathbf{L}_6](OTf)_8$.

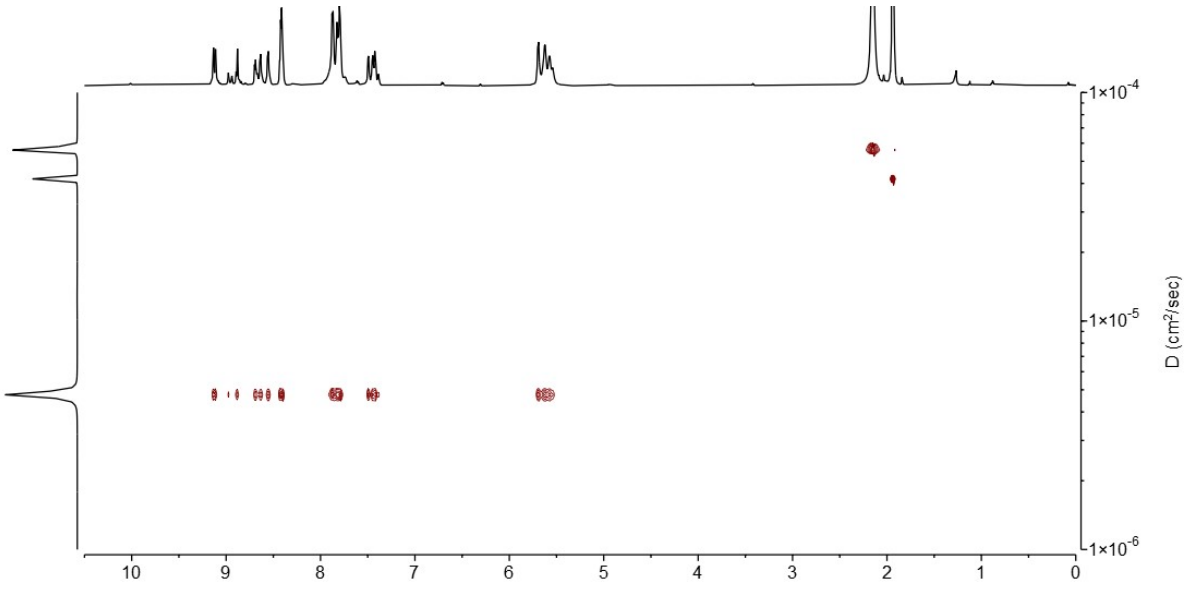

Figure S10. DOSY (700 MHz, 298K, CD_3CN) spectrum of tetrahedral cage $[Fe_4\mathbf{L}_6](OTf)_8$.

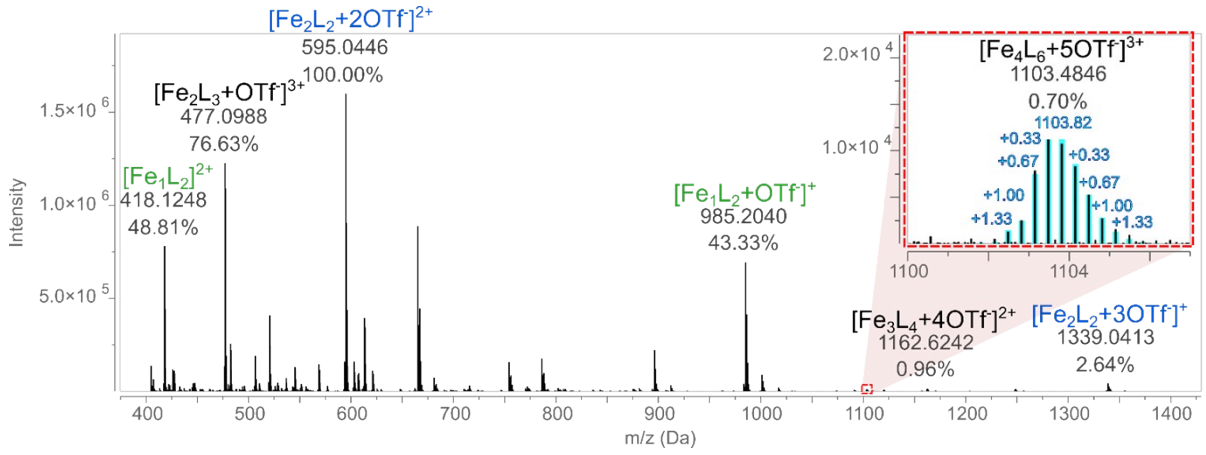

Figure S11. ESI-MS spectrum of $[Fe_4L_6](OTf)_8$. Inset: $[Fe_4L_6\,5OTf]^{3+}$ signal with theoretical *m/z* pattern (blue).

$[Zn_2L_2](NTf_2)_4$ Metallocycle

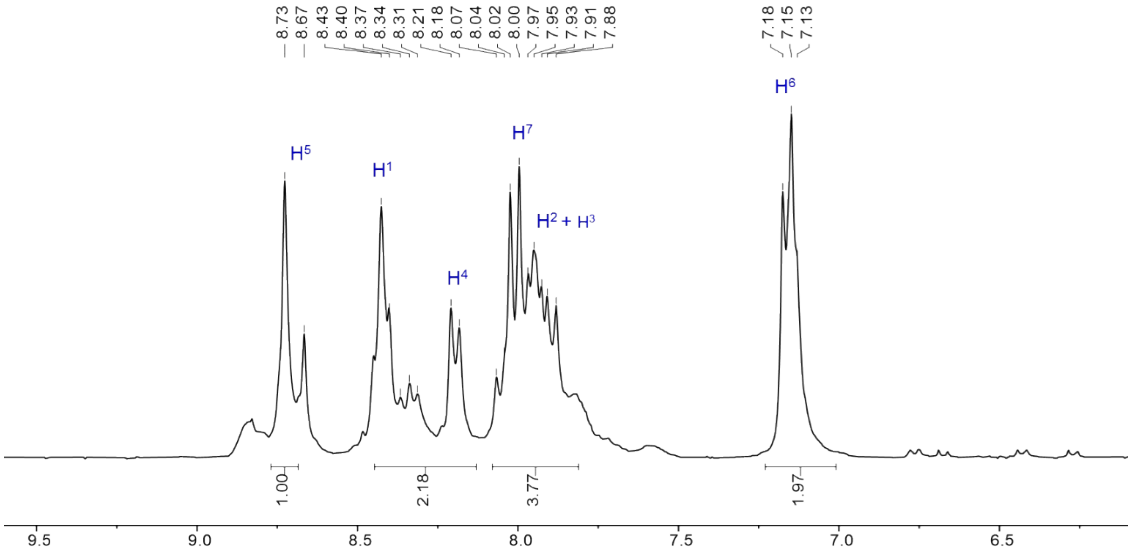

Figure S12. ^1H NMR (300 MHz, CD_3CN) spectrum of metallocycle $[Zn_2L_2](NTf_2)_4$.

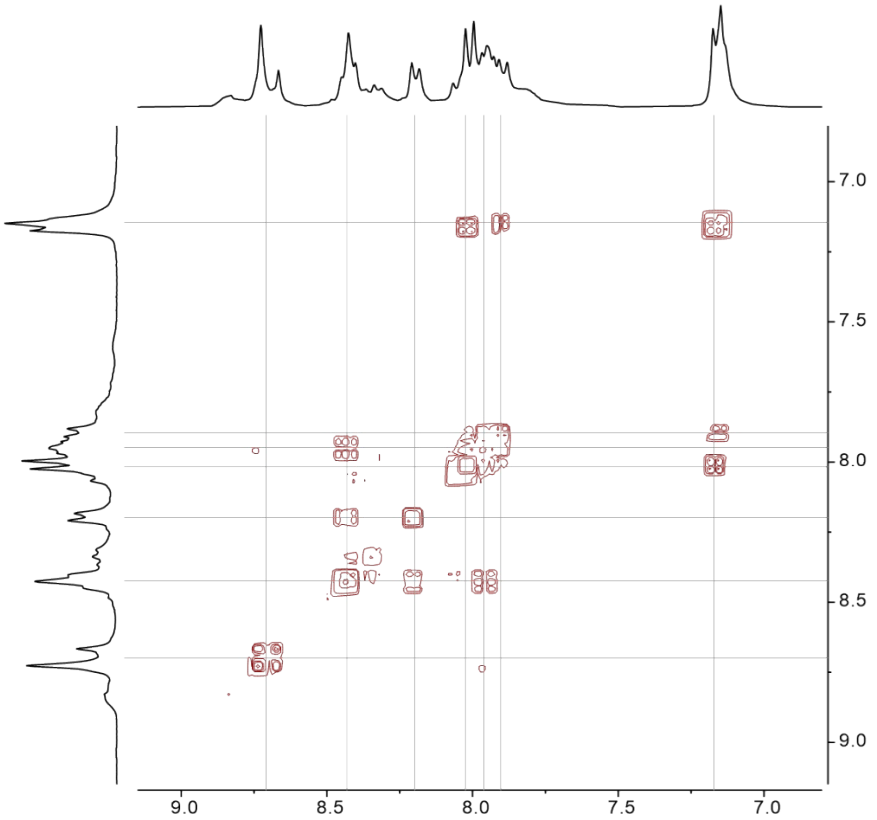

Figure S13. COSY (300 MHz, CD_3CN) spectrum of metallocycle $[Zn_2\mathbf{L}_2](NTf_2)_4$.

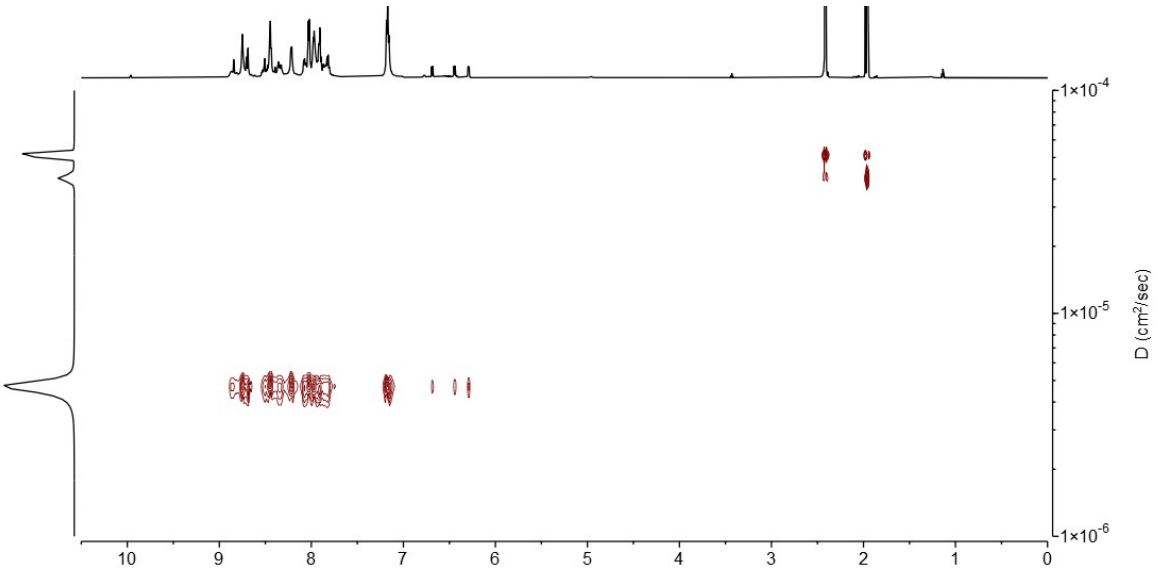

Figure S14. DOSY (700 MHz, 298K, CD_3CN) spectrum of metallocycle and cage mixture.

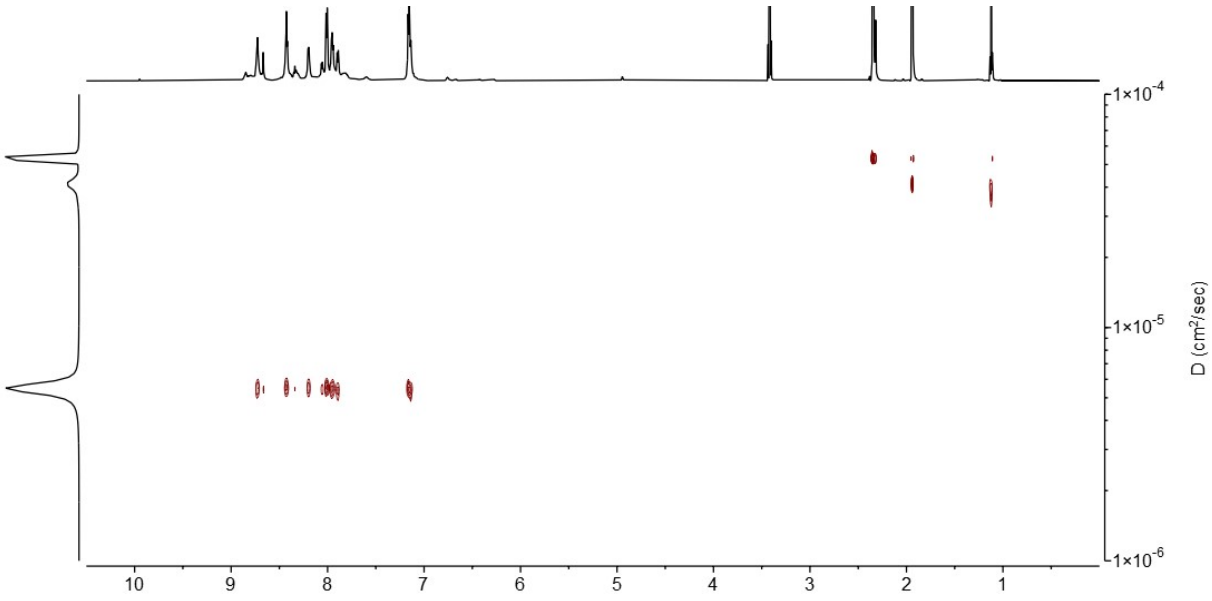

Figure S15. DOSY (700 MHz, 298K, CD_3CN) spectrum of metallocycle $[Zn_2\mathbf{L}_2](NTf_2)_4$.

$[Cd_2\mathbf{L}_2](ClO_4)_4$ Metallocycle

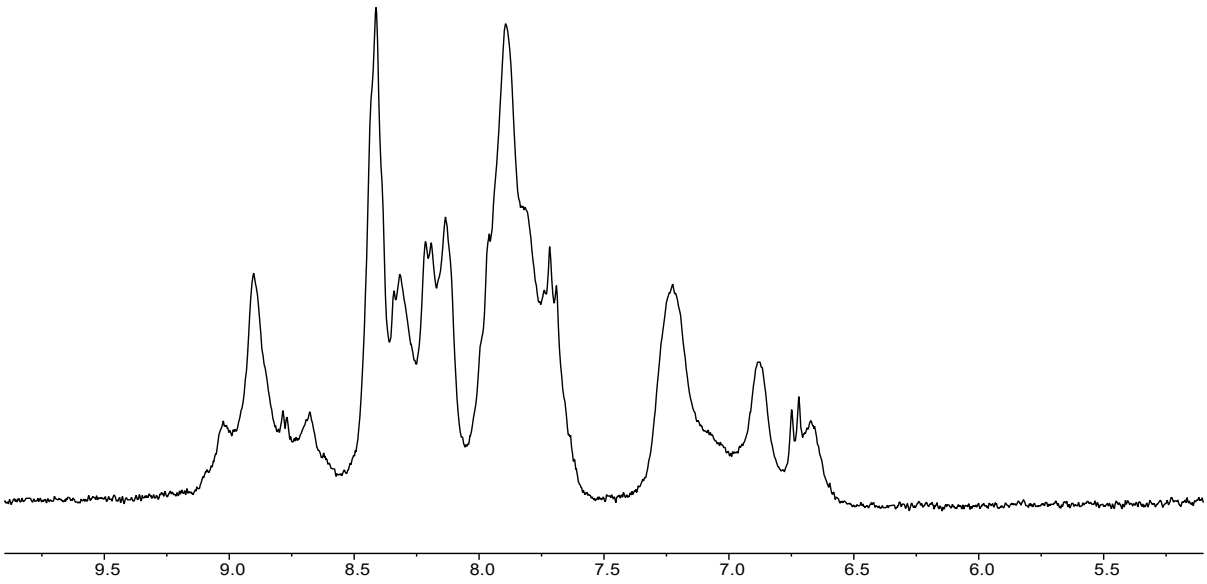

Figure S16. ^1H NMR (300 MHz, CD_3CN) spectrum of metallocycle $[Cd_2\mathbf{L}_2](ClO_4)_4$.

Structure elucidation

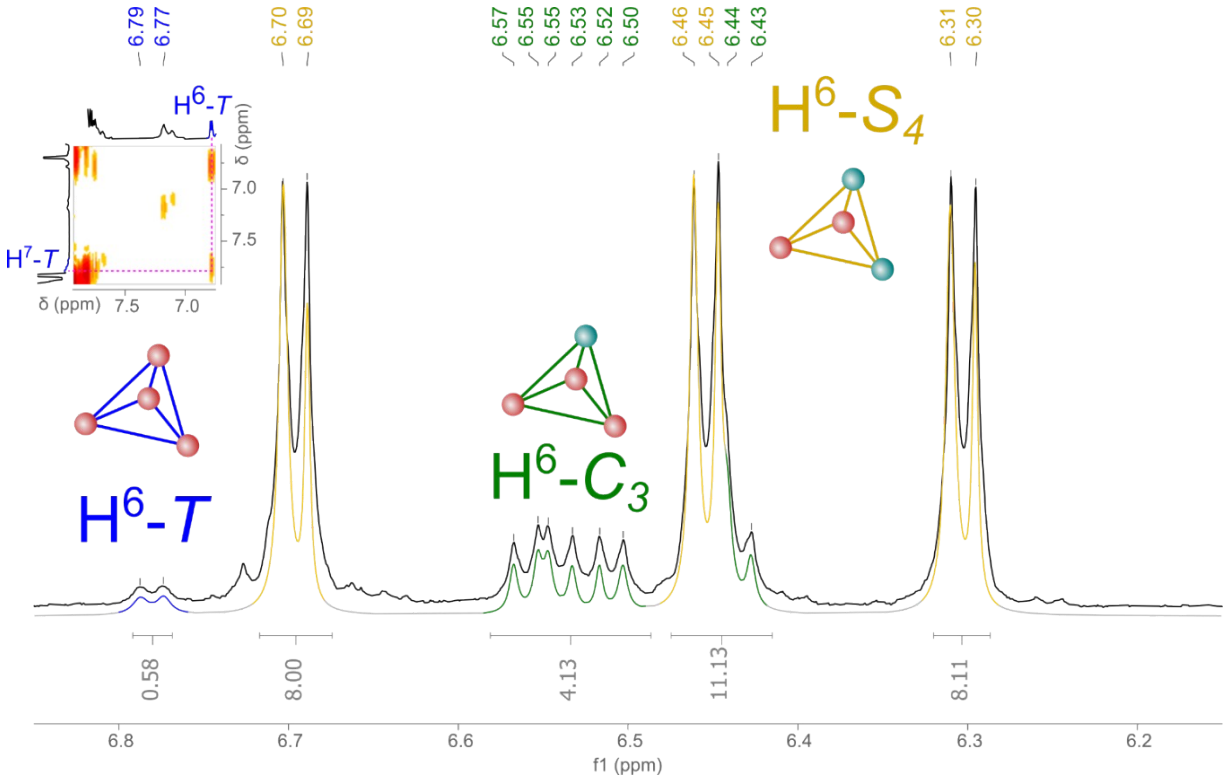

Figure S17. Deconvolution of the H^6 phenylene signal (proximal to imine bond).

Table S1. The ratio of different chiral forms of $[Zn_4\mathbf{L}_6]^{8+}$ with different counterions as obtained from deconvolution of ^1H NMR H^6 phenylene signals.

Symmetry point group	counterion				average value	standard deviation
	ClO_4^-	BF_4^-	OTf^-	NTf_2^-		
S_4	77,5%	77,3%	75,1%	77,3%	77%	1,0%
C_3	19,1%	18,3%	21,6%	20,9%	20%	1,3%
T	3,4%	4,4%	3,2%	1,8%	3%	0,9%

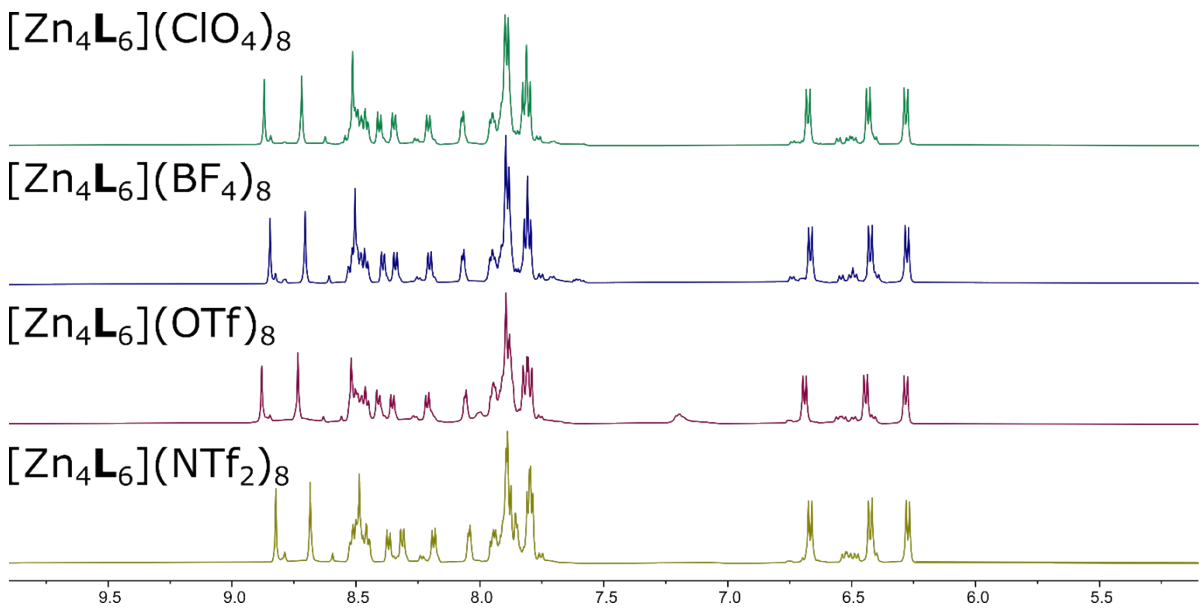

Figure S18. ^{1}H NMR (600 MHz, CD_3CN). spectra of $[Zn_4L_6]^{8+}$ tetrahedral cages with different counter ions.

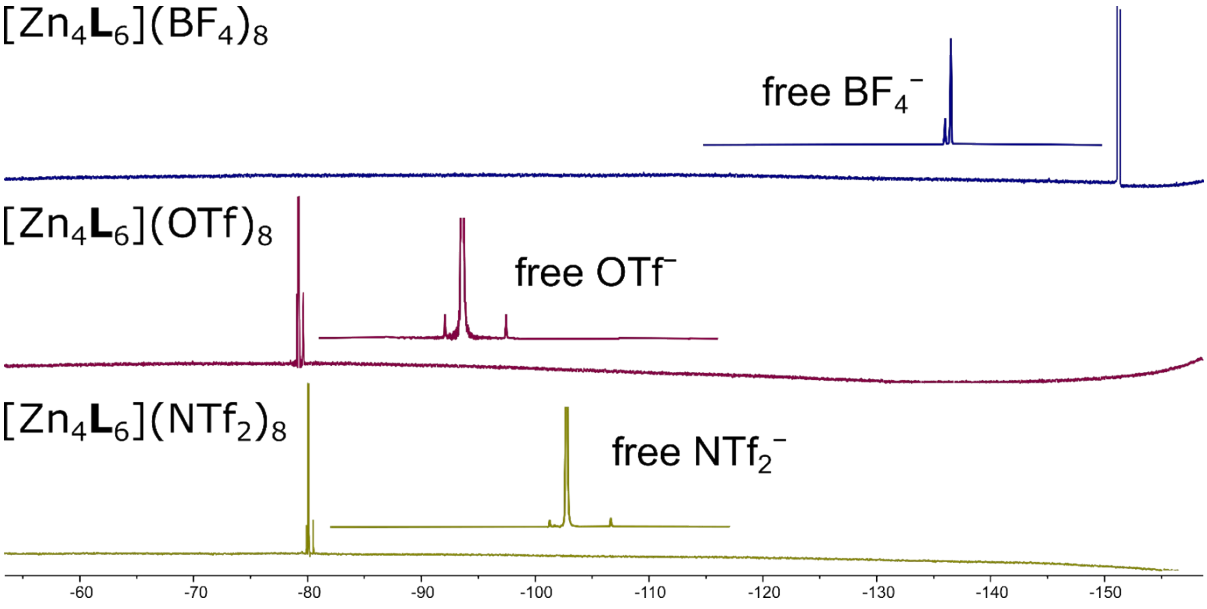

Figure S19. ^{19}F NMR (564.6 MHz, CD_3CN). spectra of $[Zn_4L_6]^{8+}$ tetrahedral cages with different counter ions.

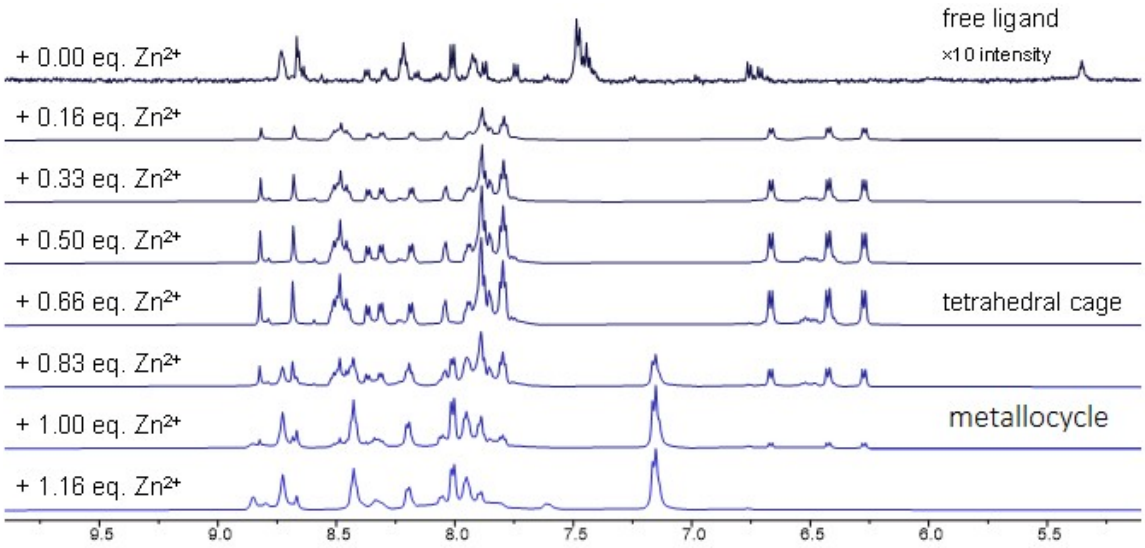

Figure S20. ^{1}H NMR titration spectra (400 MHz, CD_3CN) of *trans*-**L** with $Zn(NTf)_2$ salt solution.

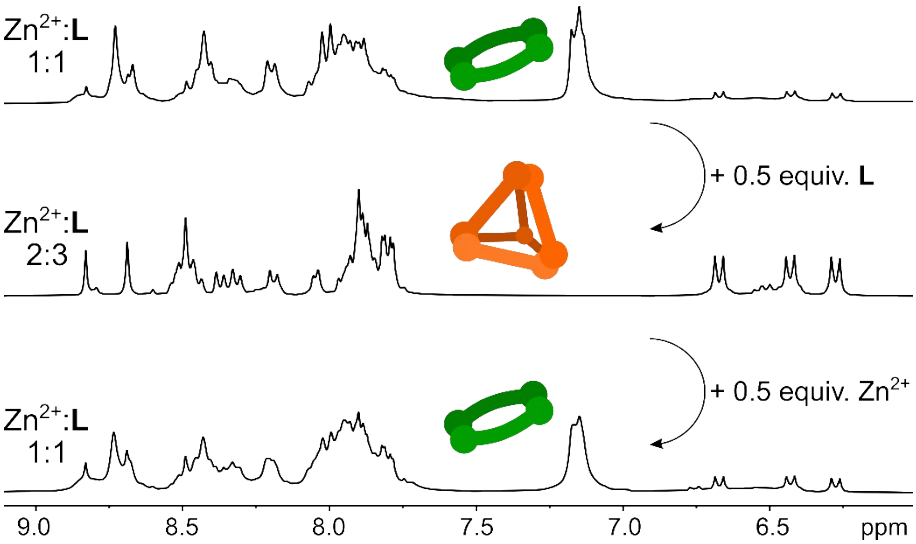

Figure S21. Switching between structures of metallocycle $[Zn_2L_2](NTf_2)_4$ and tetrahedral cage $[Zn_4L_6](NTf_2)_8$.

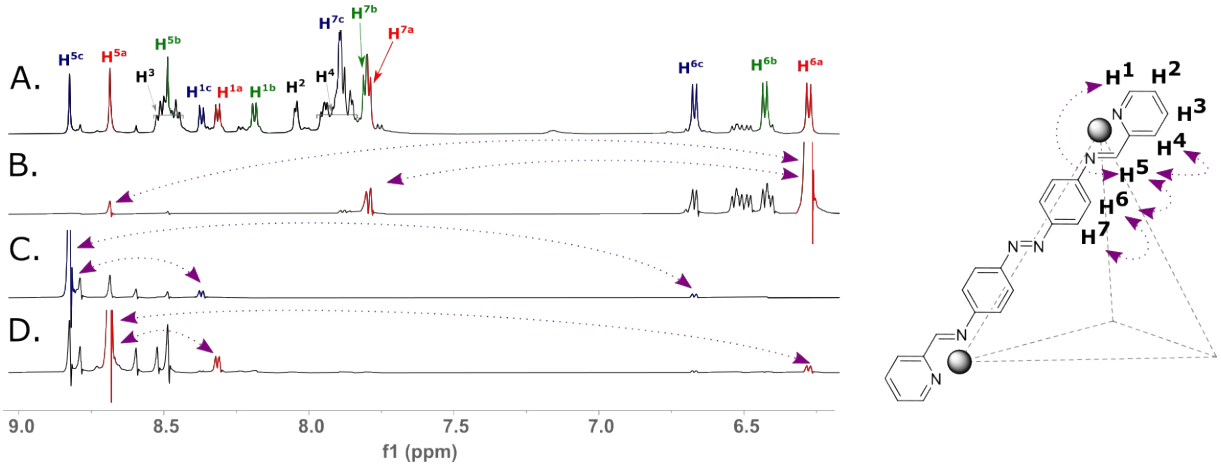

Figure S22. Selective 1D NOESY spectra (600 MHz, CD_3CN) of $[Zn_4L_6](NTf_2)_8$ tetrahedral cage.

Ligand/complex and amine/complex exchange

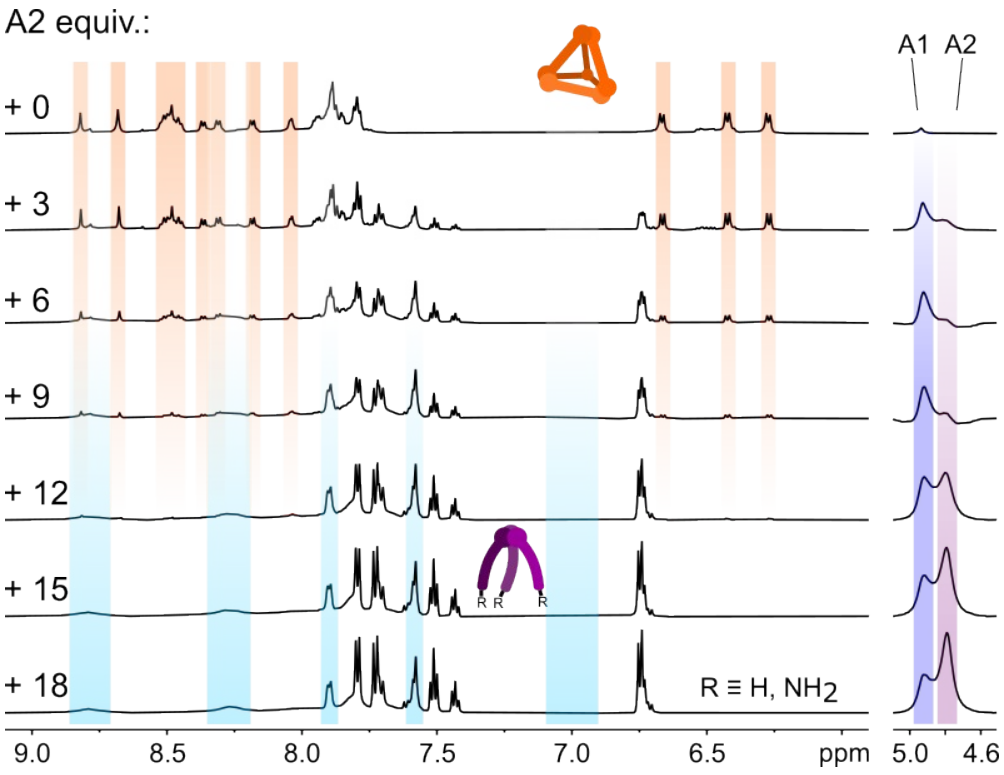

Figure S23. ^{1}H NMR (600 MHz, CD_3CN) titration of cage $[Zn_4\mathbf{L}_6](NTf_2)_8$ with 4-aminoazobenzene (A2).

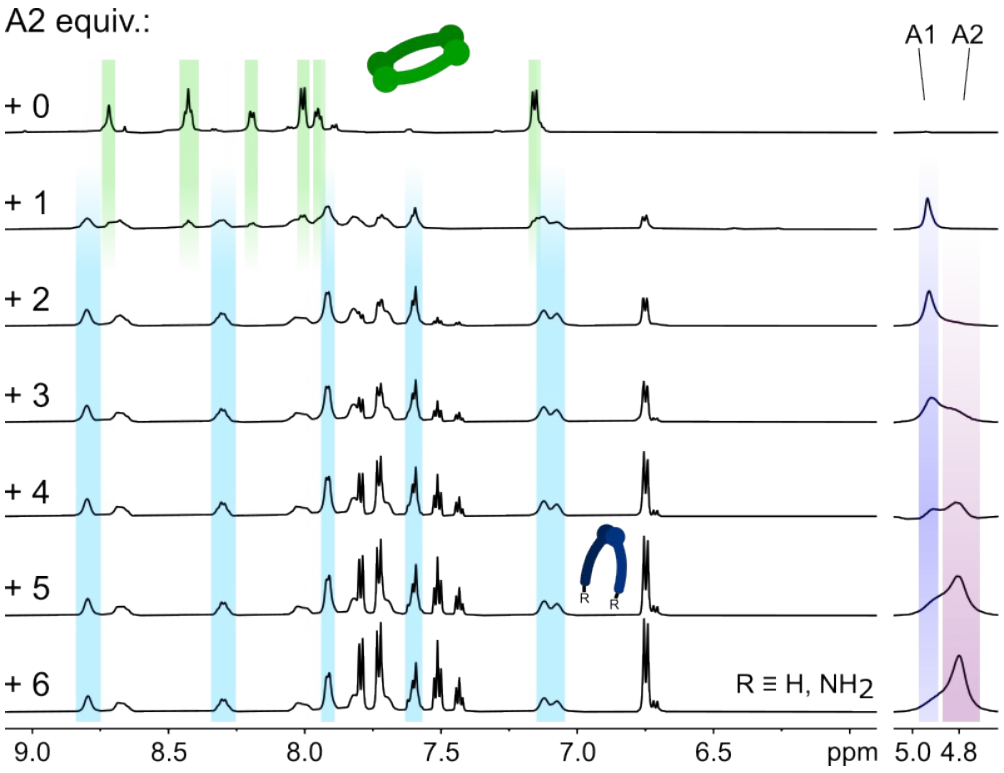

Figure S24. ^{1}H NMR (600 MHz, CD_3CN) titration of metallocycle $[Zn_2\mathbf{L}_2](NTf_2)_4$ with 4-aminoazobenzene (A2).

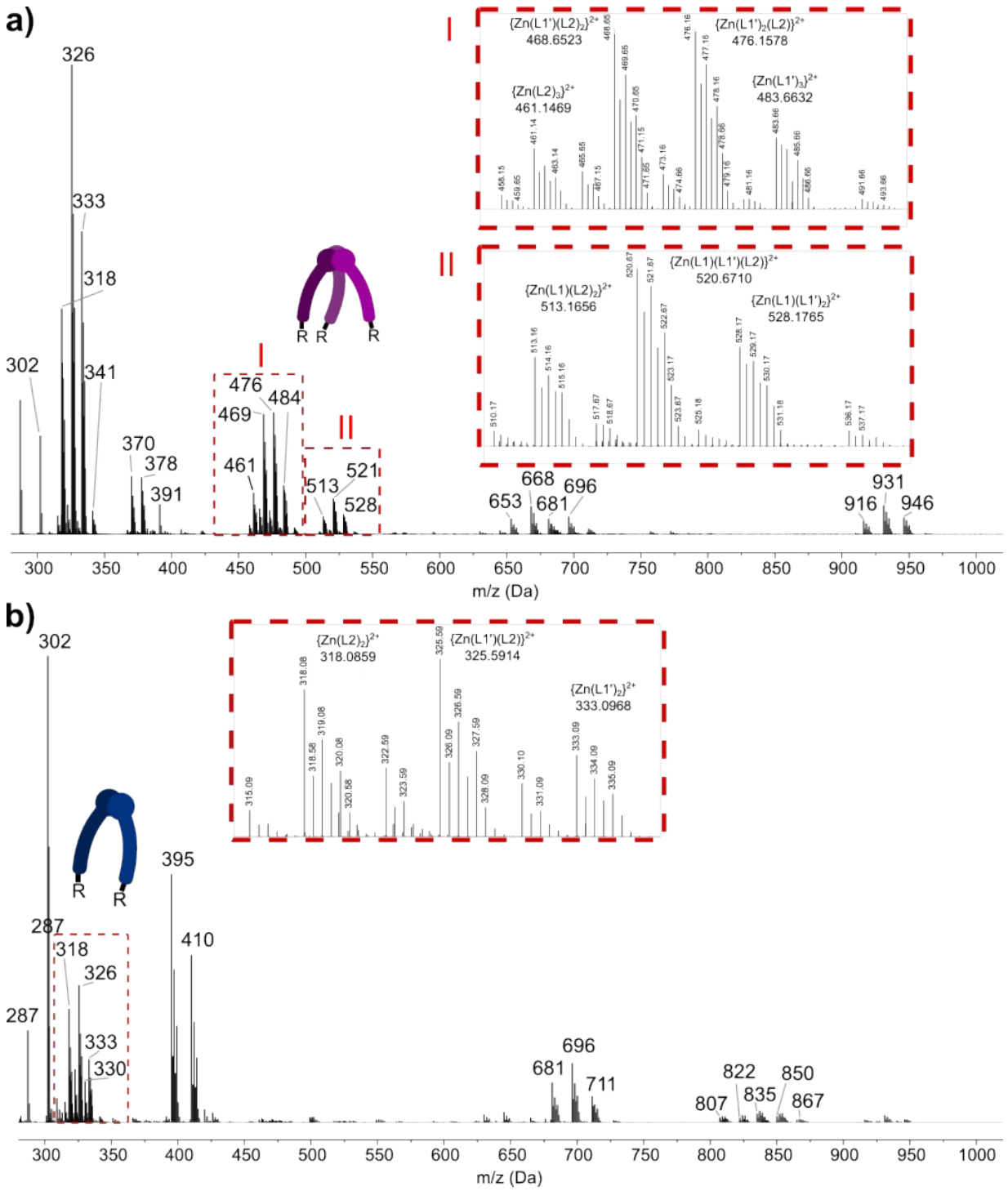

Figure S25. ESI-MS spectra comparison of mixture solutions of a) tetrahedral cage with monoamine, and b) metallocycle with monoamine. Both spectra were scaled to the same intensity. For the sake of clarity, these symbols were used in figure: L1 = **L**, L1' = **L** with single free -NH_2 group, L2 = 4-aminoazobenzene based ligand.

X-ray Crystallography

The X-ray diffraction data for $[Zn_4\mathbf{L}_6](ClO_4)_8$ and $[Zn_2\mathbf{L}_2](ClO_4)_4$ were collected on an Oxford Diffraction SuperNova diffractometer equipped with a CuKα radiation source (λ = 1.54178 Å) and with a Cryojet cooling system. For data reduction, UB-matrix determination and absorption correction, the CrysAlisPro[1] and CrysAlisRed[2] software was applied. Using Olex2[3], the structures were solved with intrinsic phasing methods employing ShelXT-2015[4] and refined by full-matrix least-squares against F^2 with the help of the SHELXL-2015[5] refinement package using least squares minimization. All non-hydrogen atoms were refined anisotropically. Some of the hydrogen atoms were derived from a difference Fourier map and they were refined isotropically. The remaining H-atoms were located in idealized positions by molecular geometry and refined as riding groups with U_{iso} (H) = 1.2 U_{eq}(C). Selected structural parameters are reported in Table S2. The data have been deposited in the Cambridge Crystallographic Data Collection (CCDC), deposition numbers CCDC 2060413 and 2060414. These data can be obtained free of charge via www.ccdc.cam.ac.uk/data_request/cif, or by emailing data_request@ccdc.cam.ac.uk, or by contacting The Cambridge Crystallographic Data Centre, 12, Union Road, Cambridge CB2.

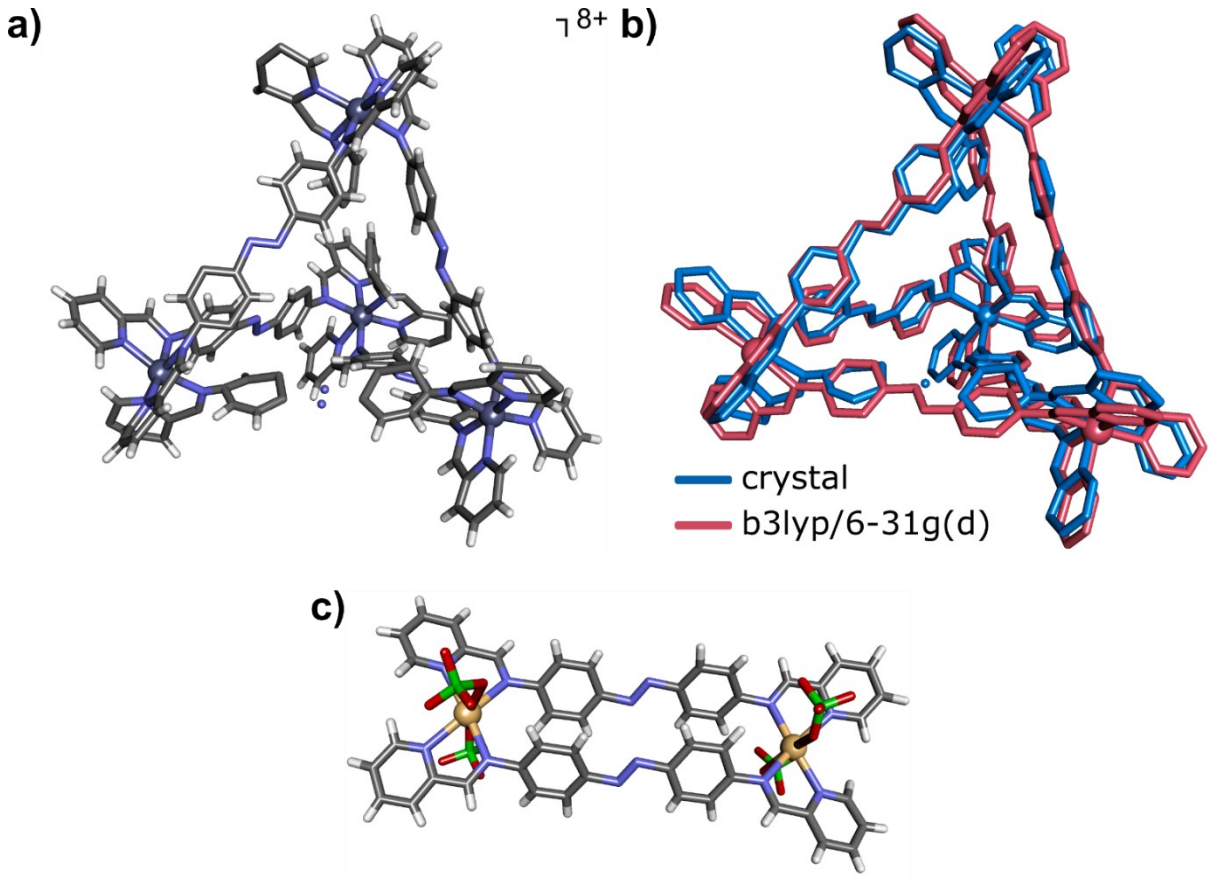

Figure S26. a) Structure of the cage cation in crystalline $[Zn_4\mathbf{L}_6](ClO_4)_8$ b) superposition of the crystallographic (blue) and DFT optimized structures (pink). c) Structure of the stoichiometric unit in crystalline $[Cd_2\mathbf{L}_2](ClO_4)_4$.\

Table S2. Crystal data and structure refinement for $[Zn_4\mathbf{L}_6](ClO_4)_8$ and $[Zn_2\mathbf{L}_2](ClO_4)_4$.

Compound	[Zn4L6](ClO4)8	[Zn2L2](ClO4)4
Identification code	2060413	2060414
Empirical formula	C144H104N34Zn4	C48H36Cd2Cl4N12O16
Formula weight	2572.09	1403.49
Temperature/K	132(11)	293(2)
Crystal system	tetragonal	triclinic
Space group	P42/n	P-1
a/Å	23.1894(12)	8.2702(3)
b/Å	23.1894(12)	13.1132(5)
c/Å	15.787(2)	16.1592(7)
α/°	90	100.321(3)
β/°	90	90.201(3)
γ/°	90	94.960(3)
Volume/Å3	8489.3(14)	1717.30(11)
Z	2	1
ρcalcg/cm3	1.006	1.357
μ/mm-1	1.038	6.943
F(000)	2652.0	700.0
Crystal size/mm3	0.2 × 0.15 × 0.01	0.1 × 0.02 × 0.01
Radiation	CuKα (λ = 1.54184)	CuKα (λ = 1.54184)
2Θ range for data collection/°	5.39 to 79.862	5.56 to 152.994
Index ranges	-19 ≤ h ≤ 19, -18 ≤ k ≤ 19, -13 ≤ l ≤ 13	-10 ≤ h ≤ 9, -11 ≤ k ≤ 16, -20 ≤ l ≤ 20
Reflections collected	22501	12922
Independent reflections	2576 [Rint = 0.1880, Rsigma = 0.0694]	6918 [Rint = 0.0274, Rsigma = 0.0384]
Data/restraints/parameters	2576/0/225	6918/0/416
Goodness-of-fit on F2	1.542	1.053
Final R indexes [I>=2σ (I)]	R1 = 0.1821, wR2 = 0.4422	R1 = 0.0350, wR2 = 0.0938
Final R indexes [all data]	R1 = 0.2255, wR2 = 0.4840	R1 = 0.0415, wR2 = 0.0988
Largest diff. peak/hole / e Å-3	0.58/-0.53	0.67/-0.41

Photoisomerization studies

Solutions for UV-Vis measurements were prepared in ambient light and additionally covered with tin foil to limit the light exposure. Then, they were equilibrated for at least 6 hours before starting the measurements. Exposure took place in a darkened room, using a UV led lamp (1W). The measurements were carried out on a spectrophotometer immediately after exposure. Measurements were taken at regular intervals until PSS was reached and up to 100 s after the first exposure to confirm the equilibrium. The maximum absorption band was determined for individual samples and the absorbance value was used to calculate the kinetics of the reaction.

The kinetics of the isomerization reaction are of the first order, so the reaction equation depending on the absorbance of the solution can be represented in the form[6]:

$$\frac{A_\infty - A_t}{A_\infty - A_0} = \exp(-kt), \#1$$

where: A_∞ – absorbance in PSS, A_t – absorbance for given time t, A_0 - initial absorbance, without irradiation and k – reaction constant.

The reaction rate constant k may be represented as sum of rates for $k_{trans\rightarrow cis}$ and $k_{cis\rightarrow trans}$. To obtain the values of k for both processes, we must assume, that other processes are negligible and k depends on excitation light intensity. Assuming first order reaction, rate of both reactions may be written as $v_{trans\rightarrow cis} = k_{trans\rightarrow cis}$ [*trans*-**L**] and $v_{cis\rightarrow trans} = k_{cis\rightarrow trans}$ [*cis*-**L**]. In equilibrium, the rates of opposing reactions are equal $v_{trans\rightarrow cis} = v_{cis\rightarrow trans}$, thus we can substitute factors and rewrite the equation as follows:

$$\frac{k_{trans\rightarrow cis}}{k_{cis\rightarrow trans}} = \frac{[cis - L]}{[trans - L]}, \#2$$

which equals to ratio of *cis*-**L** and *trans*-**L** forms in PSS, that may be obtained from absorption spectra. The latter equals to equilibrium constant in PSS, which is K = 62/48 = 1.63. The reaction follows reversible first order kinetics, with a $k = (k_{trans\rightarrow cis} + k_{cis\rightarrow trans})$ rate constant of 0.74 s^{-1} (Fig. S27b).The reaction rate constants for isomerization were found to be $k_{trans\rightarrow cis} = (Kk)/(1+K) = 0.46$ and $k_{cis\rightarrow trans} = 0.28$.

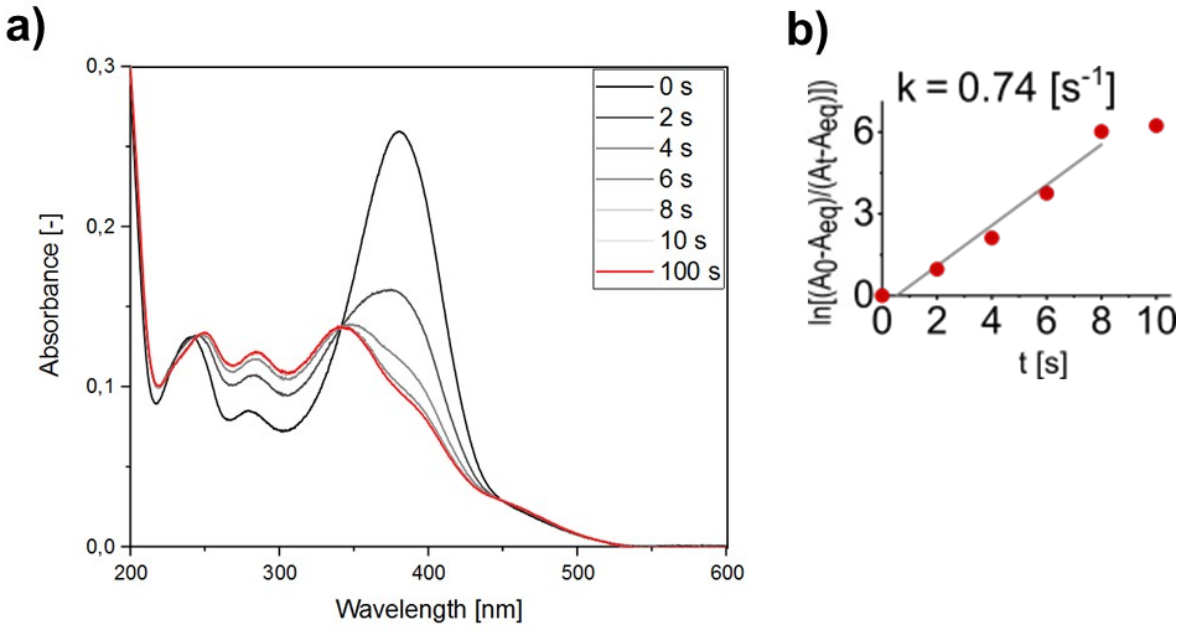

Figure S27. a) UV-Vis spectra obtained during UV irradiation of *trans*-**L** (C = 0.5·10^{-4} M, T = 298 K, CH_3CN).

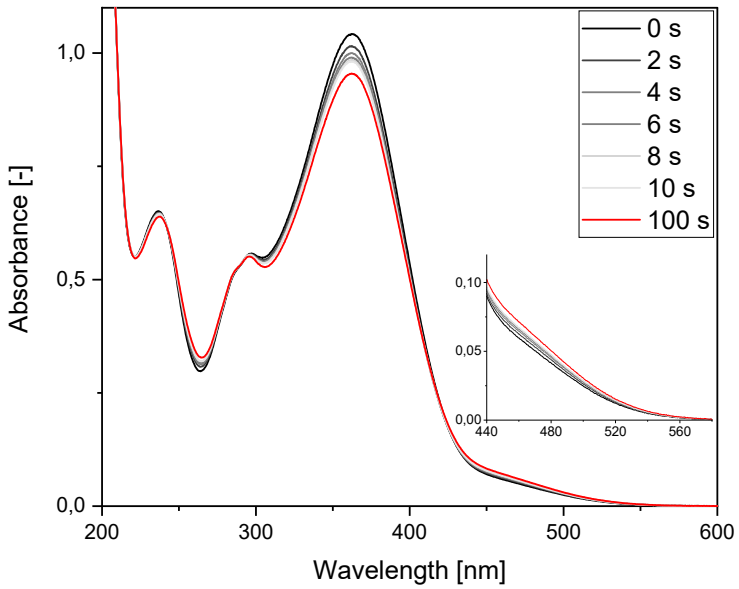

Figure S28. UV-Vis spectra obtained during UV irradiation of $[Zn_4\mathbf{L}_6](NTf_2)_8$ (C = $0.5 \cdot 10^{-4}$ M, T = 298 K, CH_3CN)

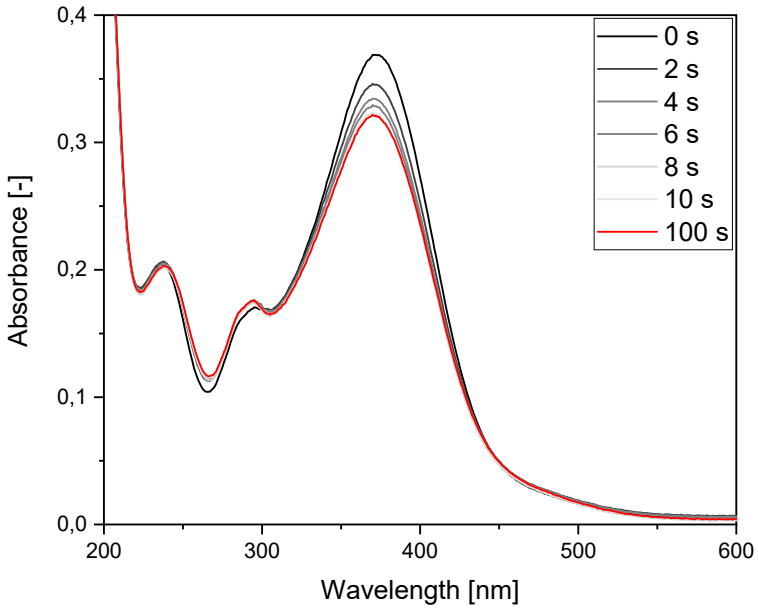

Figure S29. UV-Vis spectra obtained during UV irradiation of $[Zn_2\mathbf{L}_2](NTf_2)_4$ (C = $0.5 \cdot 10^{-4}$ M, T = 298 K, CH_3CN)

The solution of ligand was further subjected to several irradiation-heating cycles to show back and forth isomerization between *trans*-**L** and *cis*-**L**. Base solution of **L** ($c = 0.5 \cdot 10^{-4}$ M, T = 298 K, CH_3CN) was exposed to UV led lamp (1W). Each cycle consisted of heating the sample up to 348 K for 5 min, and irradiation for 1 min.

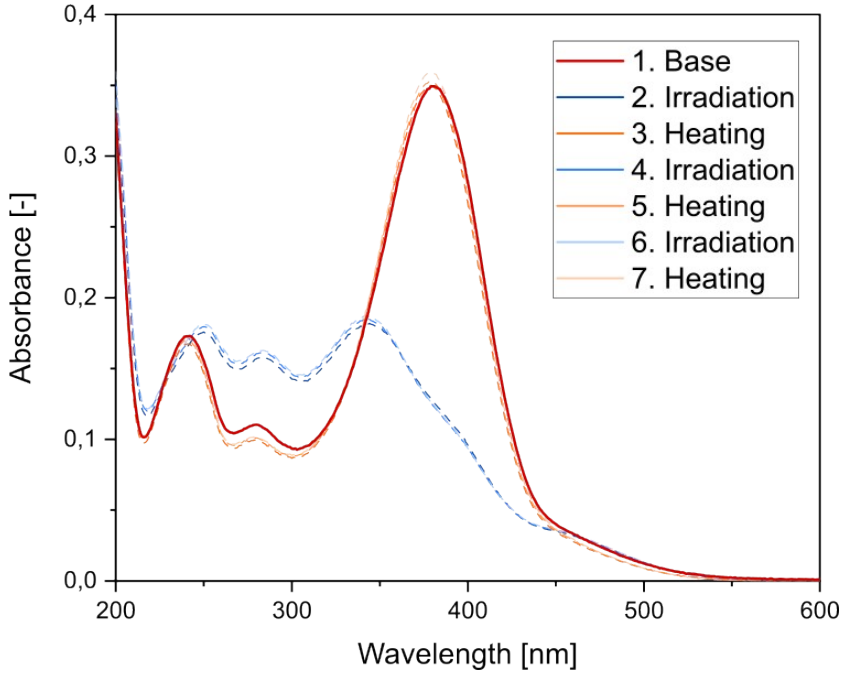

Figure S30. Photoisomerization cycles of **L** based on UV-Vis absorption spectra. ($c = 0.5 \cdot 10^{-4}$ M, CH_3CN)

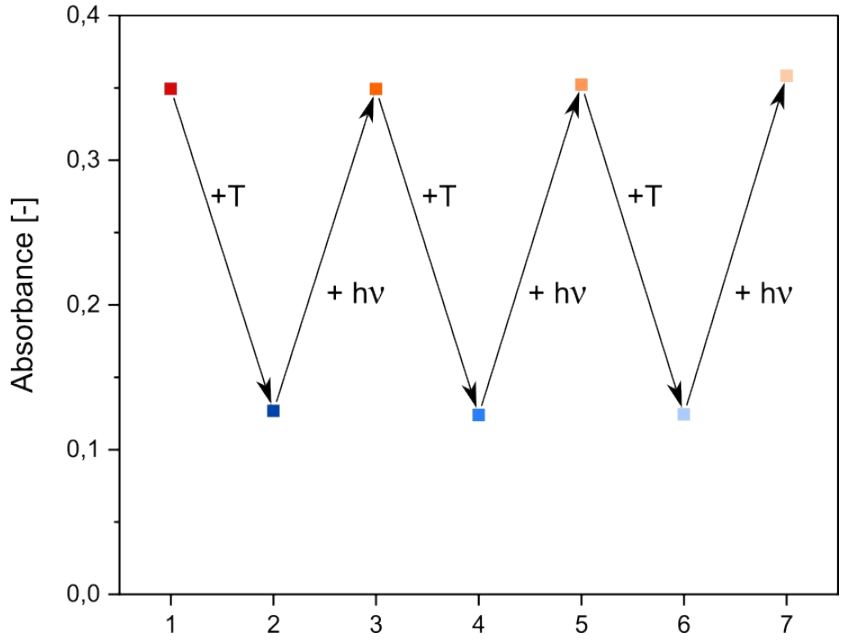

Figure S31. Photoisomerization cycles of **L** based on the UV-Vis absorption spectra. ($c = 0.5 \cdot 10^{-4}$ M, CH_3CN)

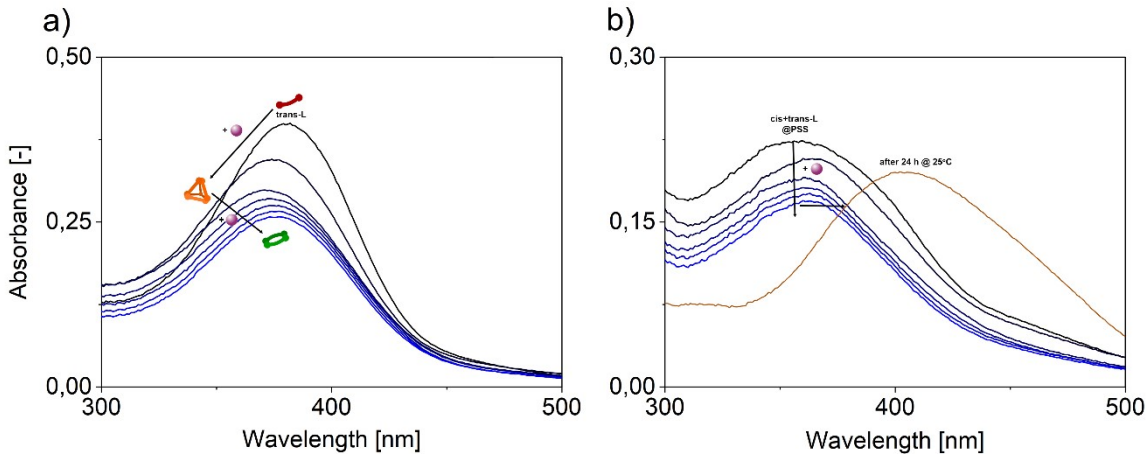

Figure S32. UV-vis titration spectra (c = 0.5·10^{-4} M, CH_3CN) of: a) *trans*-**L** with $Zn(NTf_2)_2$ solution in 0.33 equiv. increments; b) cis/*trans*-**L** mixture @PSS with $Zn(NTf_2)_2$ solution in 0.33 equiv. increments.

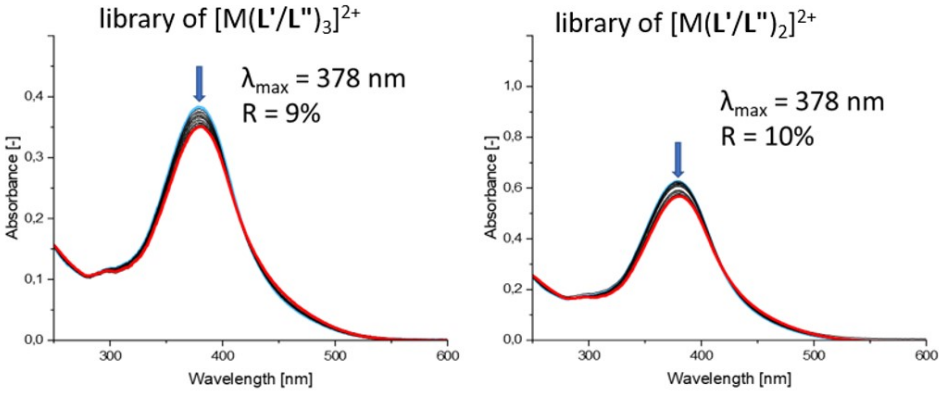

Figure S33. UV-Vis spectra obtained during UV irradiation of the libraries of $[M(\mathbf{L'/L''})_3]^{2+}$ and $[M(\mathbf{L'/L''})_2]^{2+}$ species in MeCN.

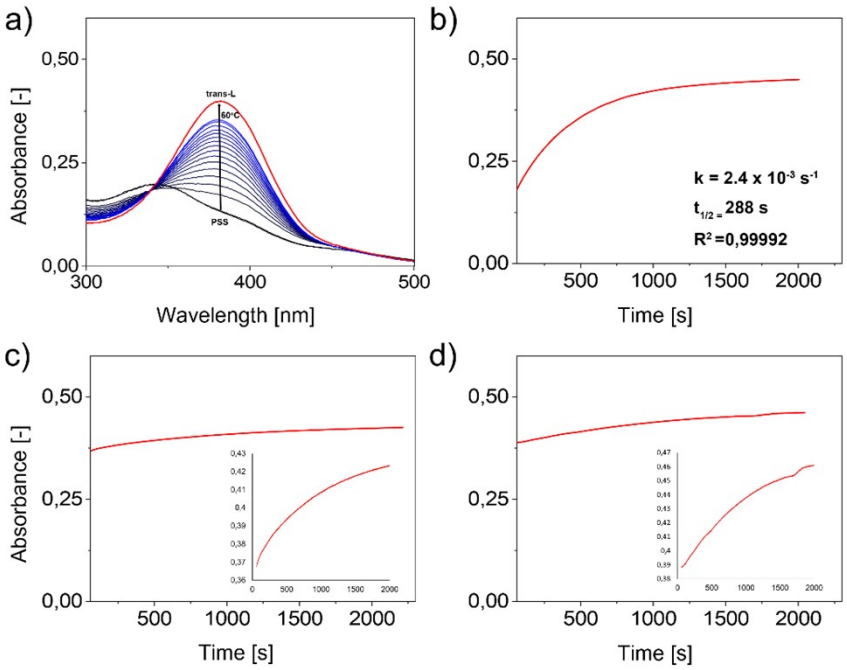

Figure S34. Thermally driven backward cis-trans isomerisation: a) UV-vis spectra recorded at 60°C in MeCN presenting cis-trans conversion of **L**. b) kinetic plot of the cis-trans conversion of **L** as monitored at 383 nm. c) kinetic plot of the cis-trans conversion of $[Zn_4\mathbf{L}_6](NTf_2)_8$ cage as monitored at 383 nm. d) kinetic plot of the cis-trans conversion of $[Zn_2\mathbf{L}_2](NTf_2)_4$ cage as monitored at 383 nm. All samples were irradiated with UV up to PSS prior the measurements.

Calculation of hydrodynamic radius

The solvodynamic radius r was calculated for the spherical diffusing species using the Stokes-Einstein equation (Eq. 2).

$$r = \frac{k_B T}{6\pi\eta D} \#2$$

where: k_B – Boltzmann constant, T – temperature, η – viscosity of solvent, D – diffusion coefficient
MeCN viscosity used for calculations: $\eta_{298\ K}=3.42\times10^{-4}$ Pa × s

Table S3. Solvodynamic radii of $[M_4\mathbf{L}_6]^{8+}$ cages and $[Zn_2\mathbf{L}_2]^{2+}$ metallocycle.

Sample[]	D [$cm^2\ s^{-1}$]	r [Å]
$[Zn_4\mathbf{L}_6](NTf_2)_8$	4.76×10^{-6}	13.41
$[Fe_4\mathbf{L}_6](NTf_2)_8$	4.76×10^{-6}	13.41
$[Zn_2\mathbf{L}_2](NTf_2)_4$	5.50×10^{-6}	11.61
mixture Zn^{2+}:**L** 1:1	4.59×10^{-6}	13.91

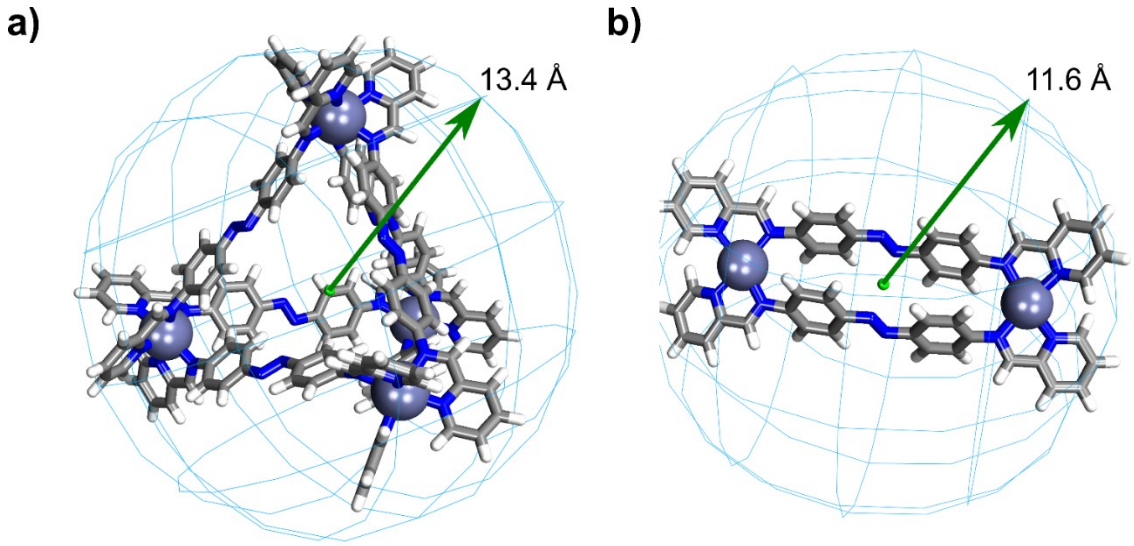

Figure S35. Tetrahedral cage and metallocycle inscribed into spheres of radii obtained from DOSY experiments.

Computational study

The calculations were performed using Gaussian 16 C.01 software and GaussView 6.1.1.[7] The structure of ligand and $[Zn_4\mathbf{L}_6]^{8+}$-T and $[Zn_4\mathbf{L}_6]^{8+}$-C_3 were optimized ab-initio, while $[Zn_4\mathbf{L}_6]^{8+}$-T and $[Zn_2\mathbf{L}_2]^{4+}$ were based on re-optimized crystal structures. The ab-initio calculations were performed in multistep regime, firstly using semi-empirical RM1 method, then re-optimized with DFT b3lyp method with 6-31g(d) basis set.

Ligand

Conformational analysis was performed for the ligand molecule using the GMMX module available in the Gaussian'16 package. In the initial search for conformers, 169 potential structures were found using the mmff94 method (energy window = 10 kcal/mol, search: 10000), 74 of which were further optimized using the b3lyp/6-31g(d) DFT method, using the implicit solvent (acetonitrile) in the PCM model. 10 unique structures were obtained in the energetic range 0 – 110 kJ/mol, of which the two lowest energetically structures are in the form of trans isomers on azo and imine bonds, and differ only in the relative position of the pyrimidine rings relative to the azobenzene plane (ΔE = 0.02 kJ/mol). Among the obtained structures, 7 assumed the *trans* conformation on the azo bond, while the remaining 3 assumed the *cis* conformation.

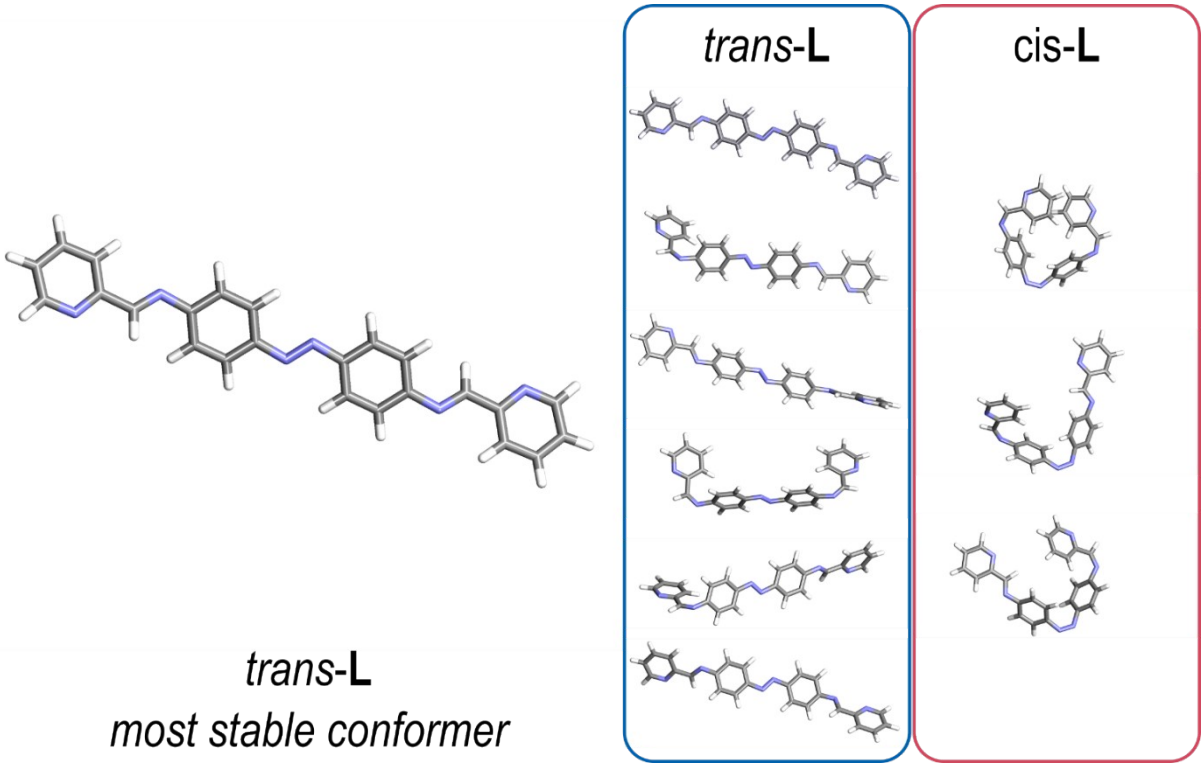

Figure S36. Most stable conformer of *trans*-**L** and other conformers found by mmff94 method and optimized using b3lyp/6-31g(d).

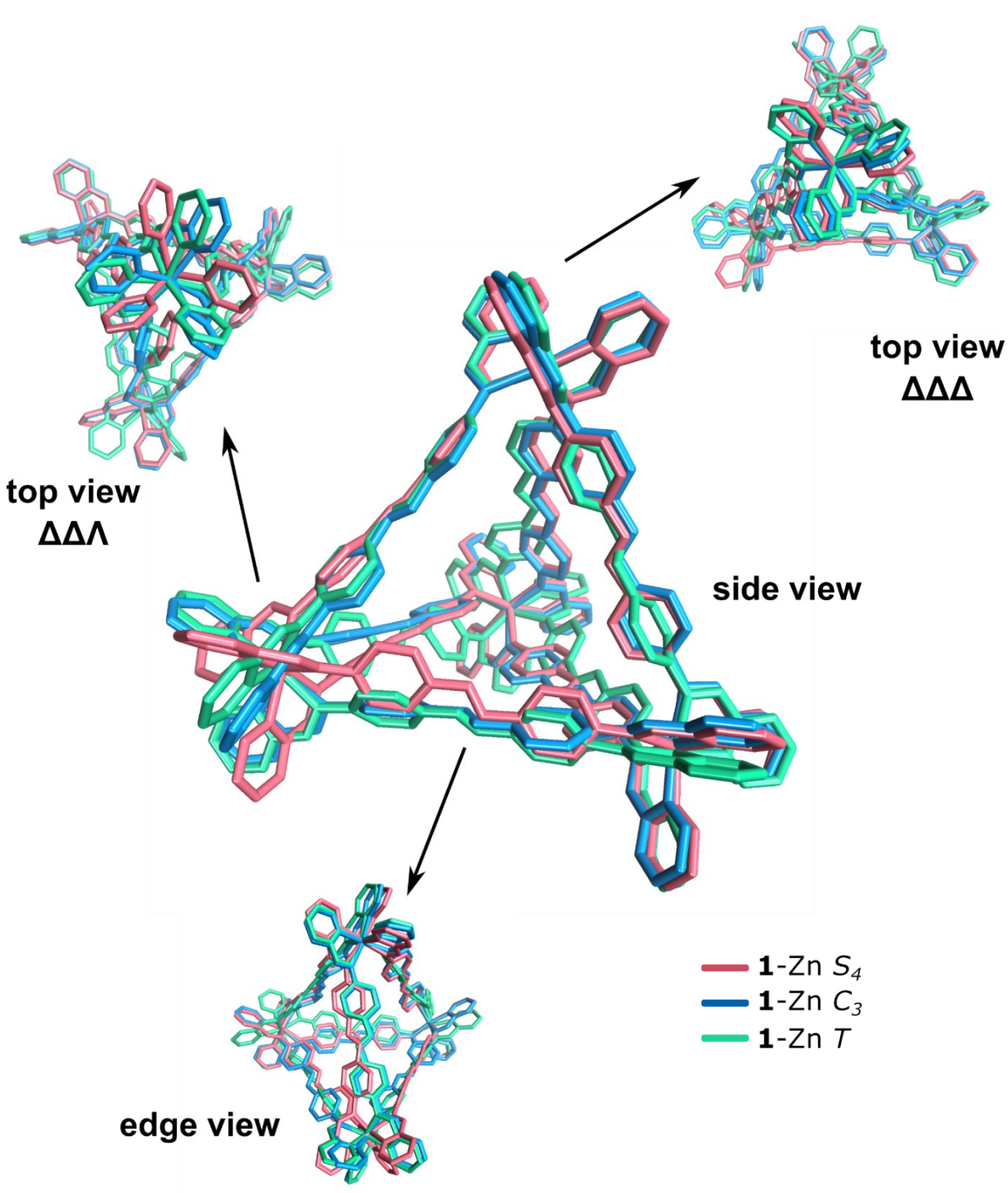

Figure S37. The superposition of different chiral forms of $[Zn_4\mathbf{L}_6]^{8+}$ (**1**) (b3lyp/6-31g(d)).

In contrast to most of the edge-bridged tetrahedral cages, $[Zn_4\mathbf{L}_6]^{8+}$ cage was found unsuited for guest encapsulation despite relatively open pores.[8] ^{19}F NMR studies have shown, that the counterions (BF_4^-, NTf^-, OTf^-) do not enter the internal cage's void (Figure S19). This might be reasoned by the fact, that both pores and the internal cavity are occupied by the highly negative electron density of azo groups (Figure S35) which prevents the encapsulation of the guests.

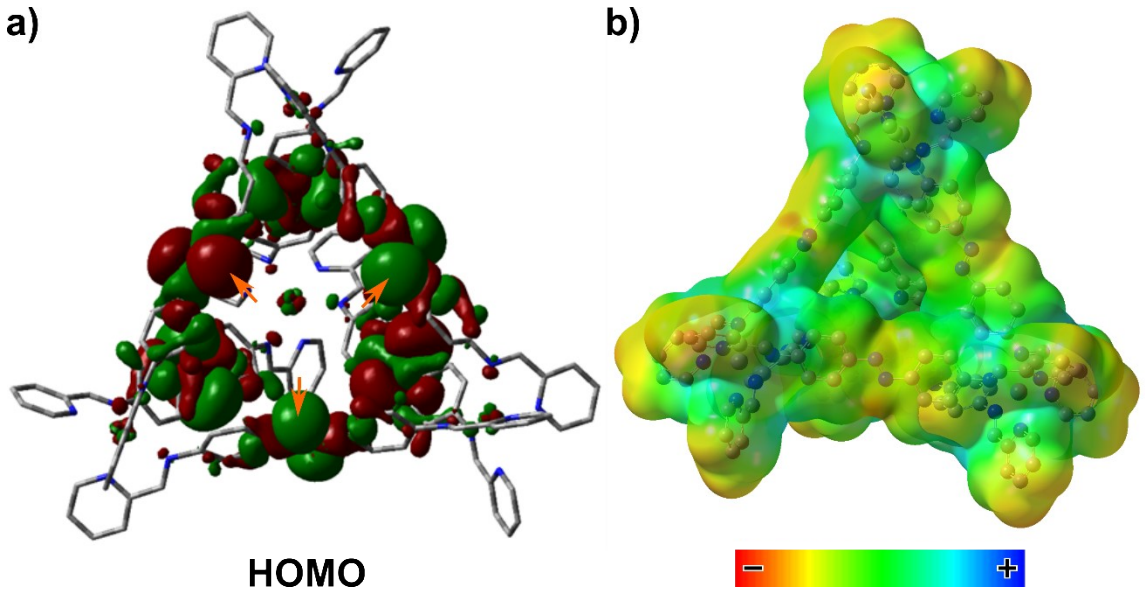

Figure S38. a) HOMO orbitals calculated (b3lyp/6-31g(d)) for cage $[Zn_4\mathbf{L}_6]^{8+}$; orange arrows show p orbitals of azo bonds on the opening of the side pore; b) electrostatic potential (ESP) shown on density surface for cage $[Zn_4\mathbf{L}_6]^{8+}$; red-coloured regions show greater negative potential localised on azo-bonds.

Metallocycle

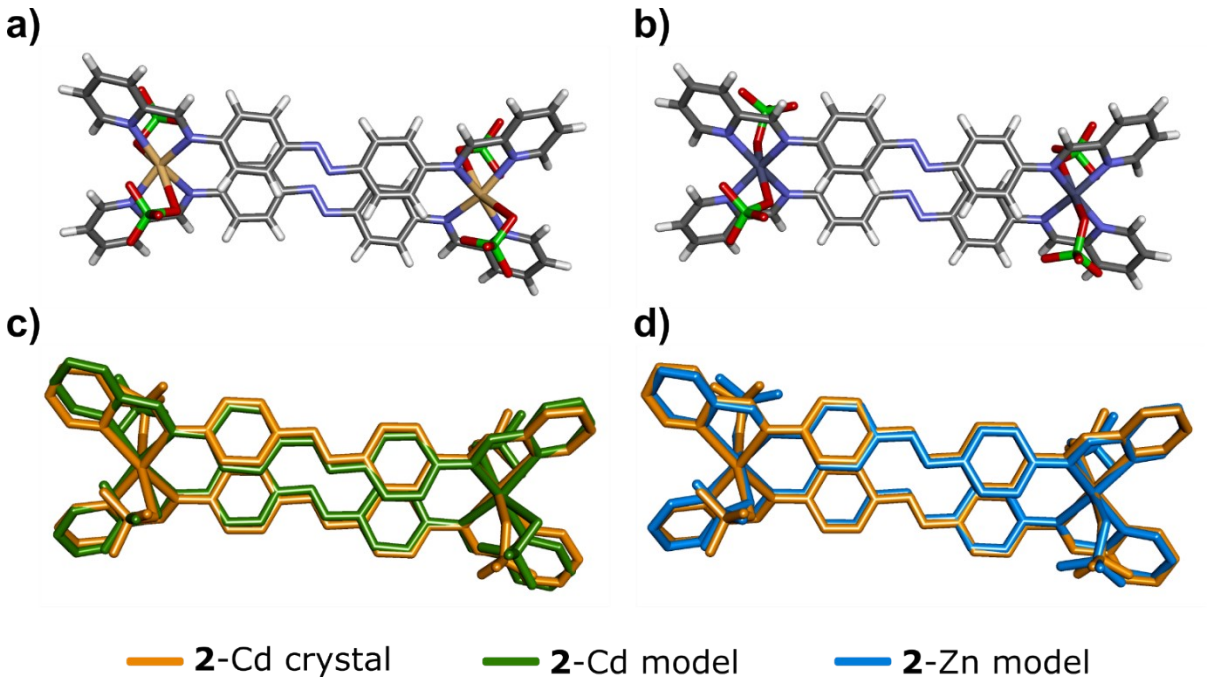

Figure S39. Optimised structures of a) $[Cd_2\mathbf{L}_2](ClO_4)_4$ (**2**) (genecp b3lyp/LANL2DZ//6-31g(d)//6-31+g(d) for atoms Cd//C,N,H//O,Cl, respectively), b) $[Zn_2\mathbf{L}_2](ClO_4)_4$ (genecp b3lyp/LANL2DZ//6-31g(d)//6-31+g(d) for atoms Cd//C,H//O,Cl, respectively). These models were superimposed with crystal structure of $[Cd_2\mathbf{L}_2](ClO_4)_4$.

References

[1] P. CrysAlis, *Yarnton, Oxfordshire, England* **2014**.

[2] C. CrysAlis, *Xcalibur PX Software, Oxford Diffraction Ltd., Abingdon, England* **2008**.

[3] O. V. Dolomanov, L. J. Bourhis, R. J. Gildea, *J. Appl. Crystallogr* **2009**, *42*, 339-341.

[4] G. M. Sheldrick, *Acta Cryst. A* **2015**, *71*, 3-8.

[5] G. M. Sheldrick, *Acta Cryst. C* **2015**, *71*, 3-8.

[6] K. Bujak, H. Orlikowska, J. G. Małecki, E. Schab-Balcerzak, S. Bartkiewicz, J. Bogucki, A. Sobolewska, J. Konieczkowska, *Dyes Pigm.* **2019**, *160*, 654-662.

[7] M. J. Frisch, G. W. Trucks, H. B. Schlegel, G. E. Scuseria, M. A. Robb, J. R. Cheeseman, G. Scalmani, V. Barone, G. A. Petersson, H. Nakatsuji, X. Li, M. Caricato, A. V. Marenich, J. Bloino, B. G. Janesko, R. Gomperts, B. Mennucci, H. P. Hratchian, J. V. Ortiz, A. F. Izmaylov, J. L. Sonnenberg, Williams, F. Ding, F. Lipparini, F. Egidi, J. Goings, B. Peng, A. Petrone, T. Henderson, D. Ranasinghe, V. G. Zakrzewski, J. Gao, N. Rega, G. Zheng, W. Liang, M. Hada, M. Ehara, K. Toyota, R. Fukuda, J. Hasegawa, M. Ishida, T. Nakajima, Y. Honda, O. Kitao, H. Nakai, T. Vreven, K. Throssell, J. A. Montgomery Jr., J. E. Peralta, F. Ogliaro, M. J. Bearpark, J. J. Heyd, E. N. Brothers, K. N. Kudin, V. N. Staroverov, T. A. Keith, R. Kobayashi, J. Normand, K. Raghavachari, A. P. Rendell, J. C. Burant, S. S. Iyengar, J. Tomasi, M. Cossi, J. M. Millam, M. Klene, C. Adamo, R. Cammi, J. W. Ochterski, R. L. Martin, K. Morokuma, O. Farkas, J. B. Foresman, D. J. Fox, Wallingford, CT, **2016**.

[8] a) T. K. Ronson, W. Meng, J. R. Nitschke, *J. Am. Chem. Soc.* **2017**, *139*, 9698-9707; b) T. K. Ronson, S. Zarra, S. P. Black, J. R. Nitschke, *Chem. Commun.* **2013**, *49*, 2476-2490; c) D. Zhang, T. K. Ronson, J. R. Nitschke, *Acc. Chem. Res.* **2018**, *51*, 2423-2436.